# EXPERIMENTAL INVESTIGATION OF SMALL CLUSTERS

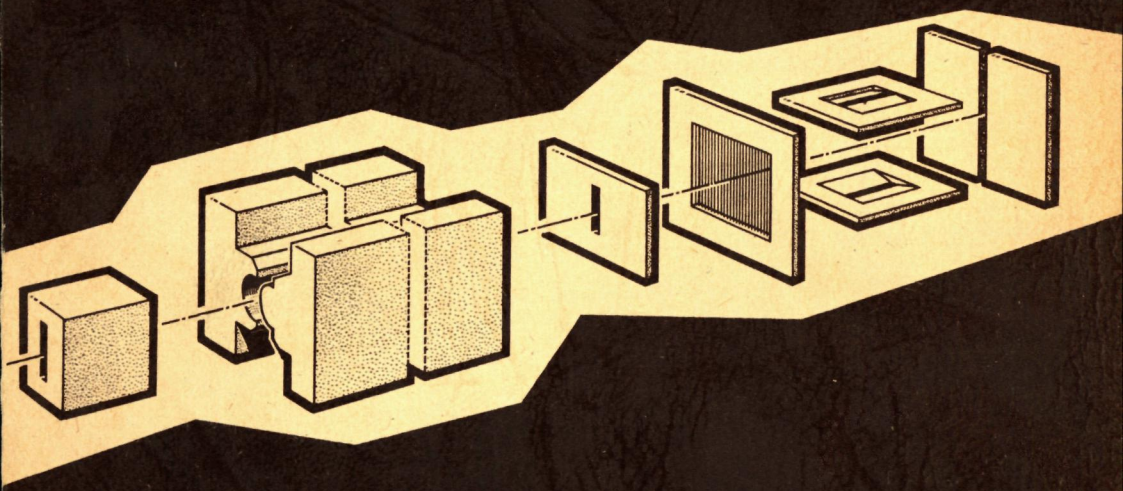

a. p. j. van deursen

No ſooner ſhe reſignes her Heart,
But from her Armes I'm forc't to part.
How can ſo hard a Fate be took,
One Night enjoy'd, the next forſook.

PROMOTORES: DR. J. REUSS
PROF. DR. A. DYMANUS

# EXPERIMENTAL INVESTIGATION OF SMALL CLUSTERS

PROEFSCHRIFT

TER VERKRIJGING VAN DE GRAAD VAN DOCTOR
IN DE WISKUNDE EN NATUURWETENSCHAPPEN
AAN DE KATHOLIEKE UNIVERSITEIT TE NIJMEGEN
OP GEZAG VAN DE RECTOR MAGNIFICUS
PROF DR A J H VENDRIK
VOLGENS BESLUIT VAN HET COLLEGE VAN DECANEN
IN HET OPENBAAR TE VERDEDIGEN
OP DONDERDAG 18 MAART 1976
DES NAMIDDAGS TE 4 UUR

door

ALEXANDER PETRUS JOHANNES VAN DEURSEN

GEBOREN TE ROTTERDAM

1976

druk drukkerij trio-print nijmegen b v -nijmegen

Velen hebben bijgedragen aan de totstandkoming van dit proefschrift. In het bijzonder wil ik bedanken

Dr. S. Stolte en Drs. A. Zandee voor de vele verhelderende discussies.

De Heren Drs. A. van Lumig en M. Waaijer voor de medewerking tijdens hun afstudeerperiode.

De Heren C. Sikkens, F. van Rijn en L. Hendriks voor hun hulp op technisch en electronisch gebied.

De dienstverlenende afdelingen, in de persoon van de Heren J. G. M. van Langen, P. C. Walraven en H. Verschoor, voor het vervaardigen van de vele onderdelen van de apparatuur en de Heer H. W. Boltze voor de stroom van vloeibare gassen.

Mej. L. v. Doorn voor het vele typewerk aan het manuscript.

De figuren en omslag zijn vervaardigd door de afdeling illustratie onder leiding van de Heer J. Gerritsen.

Het artistiek beeld van de opstelling is van de hand van de Heer L. Hendriks.

Het onderzoek, beschreven in dit proefschrift maakt deel uit van het programma van de stichting Fundamenteel Onderzoek der Materie en is mogelijk gemaakt door de financiele steun van de "Nederlandse Organisatie voor Zuiver Wetenschappelijk Onderzoek (Z.W.O.)".

Aan mijn ouders
aan Titia

CONTENTS

## 1.1. INTRODUCTION

In the beginning of this century the molecular beam technique was introduced. Molecules effuse from a source into vacuum through a small orifice. With the aid of diaphragms a minute fraction of all effusing molecules is selected to form a beam of non-interacting molecules; this beam is used for further experiments, among others the famous Stern Gerlach experiment.

In the source the pressure is held such that $d/\lambda \leq 1$; $\lambda$ stands for the mean free path of the molecules in the source, d is the orifice diameter. Optimum intensity of the beam is reached for $d/\lambda = 1$
At higher pressures the intensity levels off and the source becomes diffuse, due to the supposed formation of a cloud in front of the source; this cloud would limit the intensity, functioning as a broad virtual source. Formation of the cloud is considered uninfluenced by the pumpcapacity; its origin is attributed to collisions of effusing beam molecules amongst themselves.

In 1927 Johnson reports a continuous intensity increase for an Hg-beam, up to pressures at which $d/\lambda \simeq 1000$. The first chamber of his apparatus is pumped with a liquid air trap, a more effective pump for Hg than possible for any other gas at that moment. He attributes the intensity limitation of earlier experiments to a pressure build up in the first chamber by insufficient pumping. His experiment, however, fails to draw appropriate attention.

Some years later, Rodebush proposes a source design with a conical first diaphragm (skimmer) to avoid the cloud formation. His design, very similar to a modern nozzle source, is ignored for a long time, too. Sources are operated at $d/\lambda \simeq 1$, and the spurious cloud continues to obscure the truth.

It is 1951 when Kantrowitz and Grey propose a high pressure source, using flow conditions which can be described by continuum theory. In their design the gas is allowed to expand freely from high pressure into vacuum through a nozzle. Thereby, the thermal energy of the gas is converted into flow energy in forward direction. Orders of magnitude were promised to be gained in intensity if the $d/\lambda = 1$ barrier would be left behind. A skimmer cuts the central part out of the flow, which is transferred to high vacuum and forms a molecular beam. In 1951 a first attempt by Kistiakowsky and Slichter does not yet fulfill all expectations, although they demonstrate that higher intensities can be obtained. In 1954, Becker and Bier are able to observe the predicted increase in intensity and narrowing of velocities with the aid of larger pumps. Since then the development and understanding grows rapidly. To illustrate this, a time table is given below.

1911 Dunoyer, design of first molecular beam apparatus (Le Radium, *8*, 142)

1919 Stern and coworkers, start of a series of beam experiments (Z. Physik, *2*, 49 and *3*, 417)

1926 birth of the "cloud" (Z Physik, *39*, 764 and 780)

1927 Johnson, first free jet source, unrecognized attack on the cloud (Phys. Rev , *31*, 103)

1931 Rodebush, review of the early experiments of Stern; proposal of a source design similar to modern nozzle source (Rev. Mod Phys., *3*, 392)

1951 Kantrowitz and Grey, proposal of a continuous flow source (Rev. Sci. Instr., *22*, 328)

1951 Kistiakowsky and Slichter, first attempt with a nozzle source (Rev. Sci. Instr., *22*, 333)

1954 Becker and Bier, investigation of beams with Laval nozzle shows predicted high intensity and narrow velocity distribution. Discovery of beam seeding ($N_2$ in $H_2$) (Z. Naturforschung, *9A*, 975)

1956 Becker et al., sudden discontinuity in velocity distribution and increase in beam intensity at high pressures. First suggestion of condensation in the beam (Z. Physik, *146*, 333)

1958 First rarefied gas dynamics symposium (Nice)

1961 Bentley et al.; Henkes at al , independent reports of condensation in highly expanded nozzle beams, detection of small clusters by a mass spectrometer (Instruments and Measurements, 5th Conference, Stockholm; Z. Naturforschung, *16A*, 842)

1966 Andres, Anderson and Fenn, investigation of jets from nozzles, determination of velocity distribution in molecular beam. A study of the transition of continuum flow to free molecular flow. Velocity slip and seeding of gas mixture expanding from nozzle studied. (see J.B. Anderson in "Molecular Beams and Low Density Gasdynamics", ed. P. Wegener, M. Dekker, New York)

1966 McMichael and French , electron beam fluorescence for density measurements in the beam (Phys. Fluids, *9*, 1419)

1967 Marrone, electron beam fluorescence to determine temperature (rotational) and density in the expansion (Univ. of Toronto. Inst. Aerosp. Studies, Rep. no 113)

1969 Andres and Miller, a two dimensional Maxwell Boltzmann model to deal with the non-isotropic character of the flow for mixtures of gases (VIth RGD symposium)

Experiments with the techniques mentioned above and those in large scale wind tunnels have led to a good understanding of the flow from the nozzle orifice and the transition from continuous flow to free molecular flow. Some recent molecular nozzle beam experiments worthwhile to be mentioned (IXth. R.G.D., Gottingen) are

1974 Campargue, alternative pumping system, able to produce the beams with spead ratios $v/\Delta v$ exceeding 150

1974 Malthan and Toennies, cooling of CsF by seeding with Xe, achieved rotational temperature of 20K

1974 Winkelman and Toennies, application of Miller-Andres theory for pure gases with quantum mechanical collision cross sections

1974 Lewis et al., rotational distribution of $N_2$ in nozzle beams measured by electron beam fluorescence and laser (Raman) scattering.

Since its discovery in 1956, condensation in beams from small nozzles has had the attention of a considerable number of investigators.

1960 Becker et al., start of a series of experiments by Henkes, Hagena and Gspann and others on beams with clusters containing up to $10^6$ molecules. Cluster beams of He are produced. Cluster beams of hydrogen isotopes are proposed for thermonuclear reactions. Also studied are mass seperation effects. (†)

1963 Greene and Milne, mass spectrometric observation of small argon clusters in a nozzle beam (J. Chem. Phys. *39*, 3150)

1964 Leckenby et al., mass spectrometric detection of clusters from nozzle expansion of various gases (Proc Royal Soc A *280*, 409)

1967 Milne and Greene, careful study of the argon dimer ion signal, dependence on pressure and nozzle diameter. (J. Chem. Phys, *47*, 4095)

1967 Audit and Rouault, clusters in beams of argon analyzed by electron diffraction (C.R. Acad. Sc. Paris, *265*, 1100 B)

1969 Clampitt and Gowland, production of cluster ions of hydrogen by bombardment of solid hydrogen with ions $H^+$, $Li^+$ (Nature, *223*, 815)

1970 Milne et al., attempt to formulate a theory for dimer formation in nozzle beams (J.Chem. Phys., *52*, 1552)

1970 Golomb et al., pressure and temperature dependence of mass spectra from cluster beams of various gases (J. Chem. Phys., *52*, 1545)

1971 Herschbach et al., alkali dimers produced in nozzle expansion of pure alkali vapours (J. Chem. Phys., *54*, 2393)

1972 Foreman et al.; Klemperer et al., reactive scattering with alkali dimers; radiofrequency spectra of $(HF)_2$ (Mol. Phys., *23*, 117; J. Chem. Phys , *56*, 2442)

1974 Bederson et al., determination of polarizability of alkali dimers (J. Chem. Phys., *61*, 1816)

1974 Klemperer et al, radiofrequency spectra of dimers ArHCl and ArOCS (J. Chem. Phys., *59*, 2273 and *63*, 881)

† For a list of references, see Quarterly Report no 49, Atomic and Molecular Physics Group, Katholieke Universiteit, Nijmegen

1974 Muenter et al., radiofrequency spectra of $H_2O$ and $D_2O$ dimers (J. Chem. Phys., *60*, 2929)

1975 Bernstein et al., reactions of $(CH_3I)_n$ clusters with alkalis (J. Chem. Phys., to be published)

Alkali dimers can be separated from monomers and trimers by deflection in an inhomogenous magnetic field. In reactive scattering one can distinguish between monomers and dimers by the different kinematics. Klemperer and Muenter are able to discriminate dimers vs. larger clusters by the use of focusing fields. For atoms or molecules which have no magnetic or electric dipole moment we have to look for other characteristics, by which clusters of different size can be recognized. In most experiments involving clusters of noble gases or simple diatomics only a mass spectrometer has been used for detection. Little is known about the fragmentation which may occur in the ionization process. Due to lack of information fragmentation is often neglected completely.

## I 2 NEW INFORMATION, DESCRIPTION OF THE CONTENTS OF THIS THESIS

In the experiments described in this thesis a nozzle beam is detected by a mass spectrometer; the intensity of signals for ion masses four times the monomer mass or more is measured as a function of the source pressure $P_0$ at certain fixed temperatures $T_0$.

In chapter II which has been published in 1973, the first results are given for an $H_2$-cluster beam. The intensity of the ion signals and the velocity of the corresponding neutral clusters have been measured. At low pressures the dimer signal is masked by a space charge in the ionizer, which produces spurious dimer ion signals. With the ionizer tuned to work without space charge pure dimer signals are detected.

In chapter III, published in 1975, the intensities and cross sections for Ar-clusters are communicated; in chapter IV those for Ne, $H_2$, $N_2$, NO and $O_2$. With increasing source pressure $P_0$ all cluster ion signals appear in order of increasing mass number, m; they show a rise proportional to $P_0^{\alpha_m}$. The pressure region where this proportionality holds is called the onset region. At pressures above the onset region the signals go through a maximum. Because $\alpha_m$ is found to be independent of the source temperature $T_0$, the pressures can be scaled such that the ion intensities of each species coincide for different $T_0$. This reduction of quite a body of observational material into simple empirical plots (see fig. III.1 for instance) is a step forward compared to most earlier investigations, where this onset region was overlooked due to the use of less efficient detectors.

To be sure of the origin of the ion signals and to fill the information gap concerning the fragmentation in the ionizer, we have installed a collision cham-

ber in the neutral beam path and have determined the attenuation of the ion signals due to a scattergas. If an ion signal corresponds to a single cluster species, a constant attenuation is measured independent of $P_0$. The important outcome of our work is that this correspondence exists for dimers and monomers in the onset region. Once this correspondence had been established, the total collision cross sections of dimers can be obtained. (see chapter III and IV).

In chapter V the results for a He-cluster beam, published in 1975, are given. Signals from $He_2^+$-ions are detected. At low pressures the measurement of the total collision cross section proves that a single neutral parent is responsible for this signal; it is concluded that this parent must be a He-trimer.

For each source temperature $T_0$ a pressure $P_1$ is defined in chapter III and IV where the attenuation of the dimer ion signal starts to rise above the value which corresponds to neutral dimers. At this pressure the dimer ion signal becomes contaminated by fragments of larger clusters. Larger cluster ions appear at pressures slightly higher than $P_1$ . For Ar, Ne, $H_2$, and $N_2$ the temperature dependence of $P_1$ has been determined. Applying the principle of corresponding states a simple empirical formula is given in section IV.4.

For dimers which may possess a sufficiently large magnetic moment - those of $H_2$, NO and $O_2$–we have looked for information on this moment from the deflection of the dimers in an inhomogeneous magnetic field, see section IV.5. From the deflection of $(H_2)_2$ we infer a magnetic moment comparable to that of the monomers. For $(O_2)_2$ a deflection of 70% of the beam is observed in strong fields and for $(NO)_2$ no deflection at all. Consequently, for some investigators more unexpectedly than for others, free $O_2$-dimers possess a magnetic moment.

At pressures lower than $P_1$ only dimers and monomers are present in the nozzle beam. The question arises whether the observed dimers are already present in the source (prefabricated), or are they formed during the expansion (postfabricated)? To answer this question we have compared in chapter VI the measured dimer fraction with the calculated equilibrium fraction in the source. For Ne, Ar and $H_2$ the observed dimer fraction is in fair accordance with these calculations over a range of dimer intensities of two orders of magnitude. The diatomic systems show a temperature dependence of the dimer fraction which fits prefabrication. However, the pressure dependence does not follow a $P_0^2$ – law as expected for prefabricated dimers. Together with other experimental evidence (section VII.4) this deviation has convinced us that the dimers are actually postfabricated, as discussed in section VI.4.

The investigation of cluster beams from gas mixtures is described in chapter VII. Addition of Ar to Ne, Ne to He, and Ar to $H_2$ leads to the production of mixed dimers, NeAr, HeNe, and $H_2Ar$. Their intensity has been measured as a function of $P_0$ and their total collision cross section determined. An increase of Ar-dimers in the Ne-Ar mixture is observed with respect to the pure Ar-case, see section VII.4.

In chapter VIII we discuss the ratio of dimer to monomer cross section, $\sigma_2/\sigma_1$ as a function of reduced velocity, $v_{red} = \hbar v/\varepsilon R_m$ . The collision velocity v has been calculated under the assumption of full isentropic expansion of the nozzle beam taking into account the thermal velocity of the scattergas. The values for $\varepsilon$ and $R_m$ are taken from a Lennard Jones 12-6 interaction potential between the monomer and the scattering partner. The important feature of this plot is that in good approximation all our dimer results fall on a single curve for a large range of $v_{red}$

At low reduced velocities, $v_{red} < .4$ , $\sigma_2/\sigma_1$ is found between 1.33 and 1.45. For these velocities the total collison cross section of the monomer is dominated by the attractive part of the interaction potential $-C_6/r^6$. Assuming that this holds for the dimer too, the ratio $\sigma_2/\sigma_1$ indicates that the $C_6$–factor for the dimer interaction is about twice that of the monomer interaction.

At high reduced velocites $v_{red} \geqslant .8$, repulsive forces become of importance; the ratio $\sigma_2/\sigma_1$ reaches a value 1.9. A value $\sigma_2/\sigma_1 = 2$ would correspond to separate collisions of both monomer constituents of the dimer.

For an $H_2$-beam and Ar as scattering partner the reduced velocity ranges from $v_{red} = .24$, well in the attraction dominated region, to $v_{red} = .58$, where one enters the transition region; a gradual increase of $\sigma_2/\sigma_1$ is found.

For NO the ratio $\sigma_2/\sigma_1$ is apparently lower than for all others species investigated. This may be caused by a dipole coupling between two NO molecules; NO is the only species used possessing an electric dipole moment, but also the only species where a weak chemical binding force could be expexted.

*International Journal of Mass Spectrometry and Ion Physics*, 11 (1973) 483–489
© Elsevier Scientific Publishing Company, Amsterdam – Printed in The Netherlands

# II MEASUREMENTS OF INTENSITY AND VELOCITY DISTRIBUTION OF CLUSTERS FROM A $H_2$ SUPERSONIC NOZZLE BEAM

A. VAN DEURSEN AND J. REUSS
*Fysisch Laboratorium, Katholieke Universiteit, Nijmegen (The Netherlands)*
(First received 9 October 1972; in final form 27 December 1972)

ABSTRACT

Measurements on the production of $(H_2)_n$ clusters of small size are reported. The abundance of different clusters is found to rise to a flat maximum, at optimum source conditions for a specific cluster size. These maxima reach values of about 10 % of the $H_2^+$ signal without a strong tendency to decrease with increasing mass. The possibility of production of neutral cluster beams of known cluster size is discussed, which can be used in molecular beam scattering experiments.

## INTRODUCTION

The aim of the reported experiment has been the production of $(H_2)_n$ clusters in a molecular beam suitable for scattering experiments. Our main interest was focused on clusters of small size, in contrast to the work of a group in Karlsruhe[1] on the formation of very large $(H_2)_n$ clusters.

The production of clusters takes place during the expansion of gas flow into vacuum from a high pressure source. The temperature of the source is held a few degrees above the condensation temperature. The decisive temperature drop takes place immediately behind the source opening (nozzle) where the effusing molecules still collide with each other and where thermal energy is transformed into directed kinetic energy of hydrodynamical flow. In this region neutral clusters are formed, their sizes depending on the source conditions.

The only way to detect clusters of known size is to use a mass spectrometer equipped with an electron bombardment ionizer. However, the observed cluster ions may originate from neutral clusters of different sizes. A way to judge the origin

* This work is part of the research program of the "Stichting voor Fundamenteel Onderzoek der Materie (F.O.M.)" and has been made possible by financial support from the "Nederlandse Organisatie voor Zuiver Wetenschappelijk Onderzoek (Z.W.O.)".

of a cluster ion is to look for the pressure dependence of the signal, for a fixed source temperature. Our results show that one can adjust the source conditions such that a well-defined neutral cluster appears as parent for cluster ions of a fixed mass.

We have also investigated, whether a difference in the velocity distribution for neutral clusters of different masses could serve as a means of determining the parentage of a cluster ion. However, the velocity distributions of the clusters were nearly independent of the ion mass.

The measured relative abundances of ions show that the signals for different ion masses are influenced by the different stabilities of the cluster ions. Even masses have intensities about 50 times smaller than odd masses. Mass 4 could not be detected with certainty. Ions of masses 9 and 15 appear to be of high stability.

## APPARATUS

The molecular beam apparatus used was of conventional design. It consists of six separately pumped chambers (Fig. 1). The source chamber is pumped by a 1000 l $sec^{-1}$ jet pump with a water cooled baffle. Stable operation was obtained at pressures lower than $2 \times 10^{-3}$ torr, with the molecular beam on. The next chamber contains a beam chopper w (30 Hz, permits phase sensitive detection) and is equipped with a 2000 l $sec^{-1}$ oil diffusion pump and a water cooled baffle. The pressure measured here was always less than $10^{-6}$ torr. The following chamber accommodates the velocity selector (slotted disc type). Between the chopper chamber and the velocity selector a separately pumped chamber can be inserted containing the scatter box, "b" for total collision cross section measurements. The velocity selector is followed by a buffer chamber and the detector chamber with ionizer and mass spectrometer. The pressure in the detector chamber is $10^{-9}$ torr

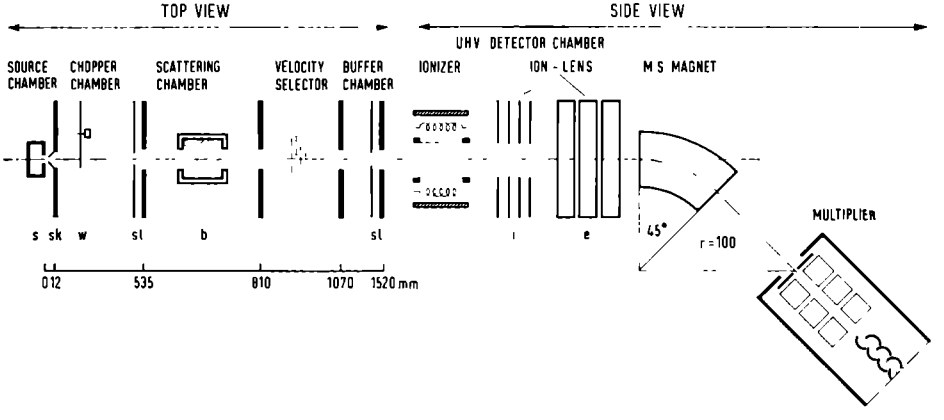


Fig. 1. Scheme of the apparatus. Heavy vertical lines indicate a division between separately pumped chambers. The detector utilizes half a sector field so that a carefully prepared parallel ion beam is needed (i = immersion-lens; e = Einzel-lens).

under working conditions. In Fig. 1 the dimensions of the whole apparatus are indicated.

During most of the measurements presented here the scattering chamber was removed. In the first chamber the molecular beam source s is mounted. The nozzle opening has a 28 $\mu$ diameter pierced into a 25 $\mu$ thick stainless steel foil by an etched molybdenum wire. The foil is held between a brass plate with a central bore of 1 mm diameter and a brass mounting base with a small rim for vacuum sealing. This base is attached to the source body, which can be cooled to about 20 °K and wherein the pressure can be varied between 0.05 and 8 atm.

The source body is made of a rectangular copper piece with an 11 mm central bore into which a shaft of sintered material is crammed in good thermal contact with the walls. The hydrogen gas flows through this sintered material accommodating to the temperature of the source body. The whole source system is mounted onto a Klipping-He-cryostat (Leybold VMK 500). Two vapour pressure thermometers monitor the temperature of the cryostat and the source body. Between the two points a temperature difference was observed which depends on the inlet pressure; at high inlet pressures the background pressure in the source chamber increases and causes higher thermal losses.

The temperature of the source was regulated between 20° and 28 °K; most measurements were made at 26 °K. Hydrogen molecules of the background gas in the source chamber intermittently condense on the cappillary through which the liquid He flows to the cryostat. Consequently, the pressure in the source chamber fluctuates and causes a varying attenuation of the molecular beam. We sealed all openings between the cold capillary and the source chamber with tape and were able to reduce the beam fluctuations below a tolerable limit. A conical skimmer sk (90° full cone angle, 0.72 mm diameter orifice) is placed 12 mm downstream from the nozzle. The skimmer forms the only vacuum connection between the first and the second vacuum chamber. Collimation of the molecular beam is achieved by two adjustable slits sl, one between the chopper chamber and the scattering chamber and one in front of the detector chamber.

The molecular beam is analysed with a small magnetic mass spectrometer developed by Stolte[2]. Its mass range is 1–40, its resolution $M/\Delta M = 40$. In the ionizer electrons of 100 eV traverse the neutral beam path. Care must be taken that the neutral beam nowhere hits the walls of the ionizer. Otherwise neutral clusters could break up and the relative values of the ion intensity at different masses would become less meaningful. The ions are detected after amplification by an open multiplier system with the conventional lock-in technique.

The gas inlet system contains two liquid nitrogen cooled traps in order to purify the source gas sufficiently. We use 96 % pure hydrogen gas which passes through the first trap whereby moisture is removed. In the second trap, which is filled with molecular sieve, the remaining nitrogen is removed. Stable operation of the nozzle is possible for more than 8 hours without clogging up.

The measurements reported in this section were all performed with the source at 26 °K. Preliminary measurements had shown that with this source temperature we got all small clusters within a convenient range of source pressures. With the source at nitrogen temperatures we were only able to detect mass 3 and mass 5 ions, the latter ones barely.

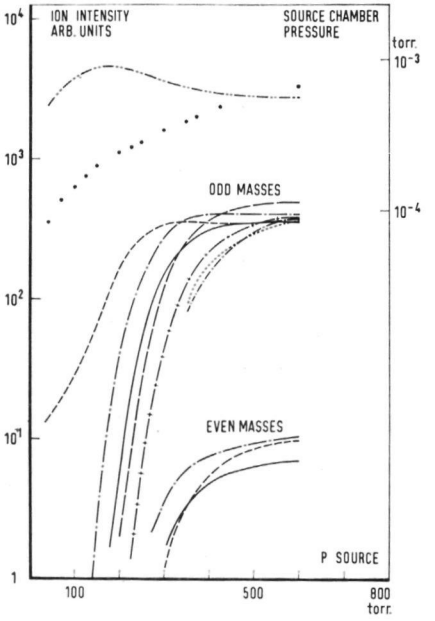


Fig. 2. Ion intensity plotted against inlet pressure. — ·· — corresponds to mass 2; ----- to mass 3; — · — to mass 5 and 6; ——— to mass 7 and 8; —— to mass 9 and 10; — + — to mass 11; ---- to mass 13 and — · — to mass 15. ····· gives the dependence of the pressure in the source chamber on the inlet pressure (scale at the right).

The intensity of the ion clusters was measured as a function of the source pressure. In Fig. 2 results are shown for $p_{source}$ between 40 and 600 torr. For reference the $H_2^+$ signal is shown, too. The odd masses reach intensities of about 13 % of the $H_2^+$ intensities, in contrast to 0.3 % for the even masses. For pressures higher than 600 torr we observed a small decrease of intensity for small clusters while the $H_2^+$ signal still rose. However, at these high pressures the background pressure in the source chamber rises to about $10^{-3}$ torr and strongly interferes with the cluster intensities by beam attenuation and possibly cluster destruction.

During the measurements the neutral beam was well collimated so that no wall collisions could occur in the ionizer. However, the entrance grid of the ionizer had an 80 % transparency so that some clusters could be broken up there leading to an enhancement of the signals for low masses. That this effect is real was shown

in an experiment where we deliberately directed the molecular beam against the exit plate of the ionizer. At source pressures of about 600 torr a relative enhancement of the $H_2^+$ signal was observed by a factor two.

The $H_3^+$ signal does not originate purely from neutral clusters bombarded by electrons. At source conditions where no condensation can be expected ($T = 300\,°K$, $p = 100$ torr), the $H_3^+$ signal still amounts to 0.5 % of the $H_2^+$ signal. In the ionizer, the reaction $H_2^+ + H_2 \rightarrow H_3^+ + H$ takes place between $H_2^+$ and incoming $H_2$ molecules producing a chopped and phase locked signal of mass 3.

This signal can also be caused partially by a modulation of the ionization efficiency. The ionization efficiency is space charge dependent and is sensitive to the modulated incoming molecular beam. In accordance with this picture we observed chopped and phase locked signals at all strong residual gas peaks.

The mass 9 signal indicates that the neutral parent cluster is formed at higher source pressures than the parent clusters for ions of smaller masses; the mass 9 signal, however, rises above all the other cluster intensities. We therefore believe that the mass 9 ion is especially stable. This conclusion gets support from the theoretical work of Huang et al.[3] from which one derives as the most probable structure an equilateral triangle ($H_3^+$) with three $H_2$ molecules positioned outside the triangle on the lines from the centre through the midpoints of the three sides. This leads to a very symmetric and, as we infer, stable structure for the mass 9 ion. In accordance with this idea the behaviour of the mass 9 signal is barely reflected by the signals from the even masses, in Fig. 2. High stability was also found from ions of mass 15 by the group of Karlsruhe[1].

Owing to the uncertainties regarding the origin of the mass 3 signal eventual scattering measurements are most meaningful for clusters measured on the masses 5, 7, 9 etc. At 150 torr the ratio of intensities for mass 5 and mass 7 is about eight. All heavier ion masses have much smaller signals. Neutral clusters with mass 8 or heavier are practically absent in the molecular beam, under these conditions, as otherwise they would show up on mass 7, 9 and higher. In consequence one can safely assume that under these particular conditions the mass 5 cluster ion originates almost entirely from a parent cluster of mass 6. Similar conditions can be found for clusters of other molecular weights.

From total collision cross sections of $(H_2)_n$ with noble gases it may be possible to determine the relative contribution of different parent clusters to the ion signal at a certain mass, for various inlet pressures. Measuerments with this aim are at present being performed in our laboratory.

## VELOCITY ANALYSIS

Our velocity selector has a resolution $\Delta v/v = 12/35$ f.w.h.m. It can be used

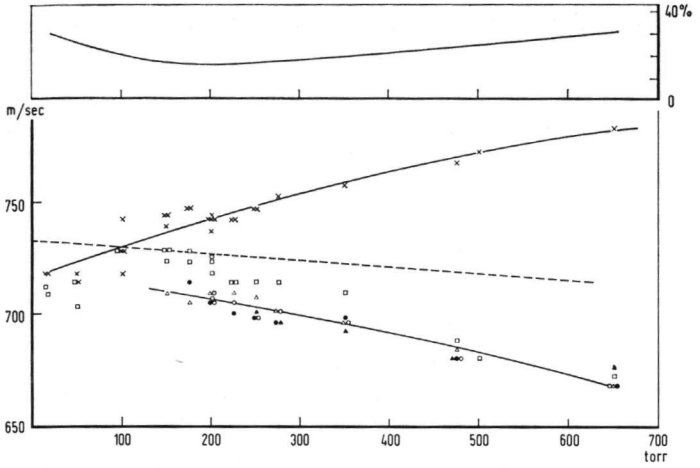


Fig. 3. Maximum transmitted velocity against inlet pressure. × are results for mass 2; □ for mass 3; △ for mass 5; ● for mass 7; ○ for mass 9; and ▲ for mass 11. The velocity spread $\Delta v/v$ for mass 5 and heavier was purely instrumental (about 37 %); a deconvoluted $\Delta v/v$ (f.w.h.m.) for mass 2 is indicated in the upper part of the figure, with the scale on the right-hand side.

to measure the most probable velocity of the beam molecules and to some extent the velocity distribution (see Fig. 3). We roughly calibrated the selector by reversing the direction of rotation. Comparing the ratio of the rotation frequencies for both directions at maximum signal (the maximum transmitted velocity) gives an estimated absolute accuracy of the velocity determination of 5 %. The relative accuracy of our velocity measurements is about 1 %.

In Fig. 3 the results of the velocity analysis are shown. The extrapolated velocity value at zero source pressure is about 715 m $sec^{-1}$. This value must be compared with 465 m $sec^{-1}$, the most probable velocity of hydrogen molecules at 26 °K, for effusive flow. Consequently, at the lowest source pressure used in our experiment we are already in the regime of a supersonic expansion.

The mass 2 signal shows a small increase with increasing source pressure. Theoretically one would expect a slight decrease as indicated by the broken line in Fig. 3. This decrease stems from the lowering of the enthalpy with higher pressures and was calculated from the discussion of the high pressure results found in ref. 4. In Fig. 3, mainly the different derivatives are of interest, in view of the 5% absolute accuracy of our measurements. The behaviour of the mass 2 signal can be understood as follows. Clusters are formed in triple collisions where two partners stick together and the lighter third partner carries away the surplus of energy. This leads to a broadening of the $H_2$ velocities as indicated in Fig. 3. Experimentally, we determine as velocity distribution the product of the velocity selector transmission and the actual distribution in the molecular beam times $1/v$ due to the velocity dependence of the detector efficiency. In this product, the

maximum transmitted velocity for a broad distribution is shifted by about 10 % to a higher value compared with a very sharp distribution.

Another influence comes from the fact that at high source pressures the background pressure rises to such values that the beam signal from the $H_2$ molecules in the vacuum chamber surrounding the source is no longer negligible. As these molecules have a higher temperature they cause a shift of the most probable beam velocity to higher values. This shift becomes more pronounced at high inlet pressures.

The velocities of the clusters measured at mass 5, 7, 9 and higher as function of the source pressure all fall on one curve. This curve has a steeper slope than follows from enthalpy considerations. We tentatively interpret this difference as a consequence of the fact that with increasing pressure the ion signal on each mass comes from parent clusters of increasing weight. These clusters are formed before the expansion is terminated, because many (triple) collisions are needed to form a large cluster. After formation of a heavy cluster it seems obvious that further acceleration by the light $H_2$ molecules falls behind in comparison to the acceleration of the $H_2$ molecules themselves. Therefore, the most probable cluster velocity is shifted towards smaller values for the heavy clusters.

Mass 3 ions show a special effect. For low inlet pressures they originate partially from $H_2^+$ ions colliding in the ionizer with $H_2$ molecules from the beam. Therefore, the mass 3 signal behaves similarly to the $H_2^+$ signal. At higher pressures, however, the fraction originating from neutral clusters is increasing. In accordance, the mass 3 signal tends to join the curve of the heavier cluster ions.

REFERENCES


1 K. Buchheit and W. Henkes, *Z. Angew. Phys.*, 24 (1968) 191.
2 S. Stolte, *Thesis*, Nijmegen, 1972.
3 J. J. Huang, M. E. Schwartz and G. V. Pfeiffer, *J. Chem. Phys.*, 56 (1972) 775.
4 J. O. Hirschfelder, C. F. Curtiss and R. B. Bird, *Molecular Theory of Gases and Liquids*, Wiley, New York, 1964.

*International Journal of Mass Spectrometry and Ion Physics*, 18 (1975) 129–135
© Elsevier Scientific Publishing Company, Amsterdam – Printed in The Netherlands

# III INTENSITIES AND CROSS-SECTIONS OF Ar CLUSTERS IN A MOLECULAR BEAM*

A. VAN DEURSEN, A. VAN LUMIG AND J. REUSS
*Katholieke Universiteit, Fysisch Laboratorium, Toernooiveld, Nijmegen (The Netherlands)*
(Received 22 April 1975)

ABSTRACT

Ar-cluster beams were produced by supersonic expansion under various source conditions. The experimental intensities have been scaled such that universal curves are obtained, up to moderate source pressures The ratio of dimer/monomer cross-sections has been determined.

## INTRODUCTION

Results of a molecular beam experiment with argon clusters are presented; special attention is given to dimers. Intensities of supersonic Ar beams with partial condensation have already been measured and interpreted by other workers [1–3] using mass spectrometry to analyse the beam In the present work the emphasis is put on the determination of the total collision cross-section as a function of the stagnation pressure, $P_0$, and stagnation temperature, $T_0$ Pressures $P_0$ range from 20 to 6000 torr, at the four temperatures 294, 223, 173 and 123 K. The nozzle is made by piercing a 30 $\mu$m diameter hole ($d$) into a 25-$\mu$m thick stainless steel foil.

The apparatus has already been described in detail [4]. The magnetic mass spectrometer has a mass range up to about 160 a m u. The electron energy in the ionizer is fixed at 100 eV. The ionizer is tuned to work without any detectable ion space-charge in the ionization volume, thus ion–molecule reactions of the incoming beam with ions can be practically ruled out. In front of the ionizer the beam is collimated by a rectangular slit with an aperture of $0.4 \times 12$ mm$^2$.

* This work is part of the research program of the "Stichting voor Fundamenteel Onderzoek der Materie (F O M )" and has been made possible by financial support from the "Nederlandse Organisatie voor Zuiver Wetenschappelijk Onderzoek (Z W O )".

The distance between the source and the detector is 205 cm. Because the ionizer has a high detection efficiency, we were able to extend our measurements to lower values of $P_0 d$ as compared to previous works [1–3].

## MEASURED INTENSITIES

Intensities were measured for the ion masses 40, 80, 120 and 160. In a log–log plot (Fig. 1) each ion signal shows a rise in the onset region proportional to ${P_0}^{\alpha m}$; $\alpha_m$ is different for different ion masses, but independent of the temperature $T_0$ over the range investigated. Values for $\alpha_m$ are given in Table 1.

For different temperatures $T_0$, the stagnation pressure $P_0$ can be scaled by ${T_0}^{\beta m}$ so that for each ion mass the intensities are represented by a single curve (see Fig. 1). Values of $\beta_m$ for different ion masses are shown in Table 1.

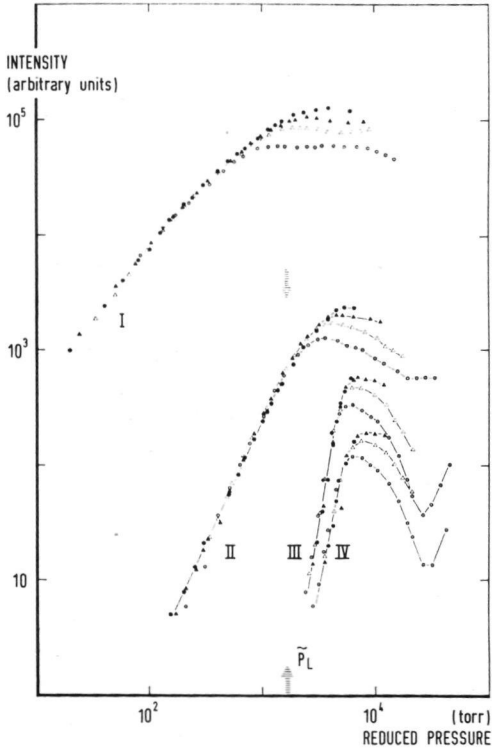


Fig. 1. Intensities vs. reduced stagnation pressure. I corresponds with the $Ar^+$, II with the $Ar_2^+$, III with the $Ar_3^+$ and IV with the $Ar_4^+$ signal. Measurements were done at source temperatures $T_0 = 294$ K (●), 223 K (▲), 173 K (△) and 123 K (○). No scaling is applied on the ordinate for different $T_0$; the pressures, however, are multiplied by $(294/T_0)^{\beta m}$. The values for $\beta_m$ are different for the four curves and are given in Table 1. Above the reduced pressure $\tilde{P}_L$ the $Ar_2^+$ signal becomes contaminated by fragments from larger clusters – see Fig. 2.

TABLE 1

VALUES FOR THE EXPONENT $\alpha_m$ AND $\beta_m$[a]

| $m$ | $\alpha_m$ | $\beta_m$ | $\alpha_m\beta_m$ | $\alpha_m\beta_m-0.5$ | $\alpha_m(G)$ |
|---|---|---|---|---|---|
| 1 | 1.1 ±0.1 | 1.05±0.15 | 1.2 | 0.7 | 1.1 |
| 2 | 2.15±0.1 | 1.9 ±0.1 | 4.1 | 3.6 | 2.5 |
| 3, 4 | 5.5 ±0.5 | 2.2 ±0.1 | 12 | 12 | 3.6 |

[a] In the onset region the signal of $Ar_m^+$ ions varies with $P_0^{\alpha m}$ at a fixed temperature. For different temperatures the signal is proportional to $P_0^{\alpha m} \cdot T_0^{-\alpha_m \beta_m}$. The exponent $(-\alpha_m \beta_m)$ of $T_0$ should be replaced by $(-\alpha_m \beta_m + 0.5)$ if neutral beam intensities instead of neutral beam densities are considered. The values $\alpha_m(G)$ derived from ref. 1b, Fig. 7, are given for comparison.

The intensities in Fig. 1 are presented as a function of a reduced pressure $\tilde{P}_0 = P_0 \cdot (294/T_0)^{\beta m}$. The measured intensities are seen to be proportional to $P_0^{\alpha m}/T_0^{\alpha m \beta m}$ in the onset region. The exponent $\alpha_m \cdot \beta_m$ must be decreased approximately by 0.5 when the intensity is to be expressed as beam flux instead of beam density.

At higher stagnation pressures all intensities go through a maximum. For $m/e = 40$ (the argon monomer signal) this can be attributed to an increased loss of particles due to condensation. Not only are argon atoms swallowed up by the condensating clusters but also other atoms acquire extra momentum from the heat of condensation and will escape from the collimated beam. At corresponding stagnation conditions an increase in forward velocity [1b] and a sudden rise in effective source diameter [5] has been observed.

For the maximum of the dimer signal, scaling factors for cluster beams of argon are available [1b]. However, we prefer a scaling for the intensity in the onset region of the dimer ion signal because effects due to heavier clusters are small there, as will be discussed below.

The pressure dependence of the different ion signals at constant $T_0$ was derived from the work of Golomb et al. [1b] and is shown in the last column of Table 1. The apparent disagreement with our results is due to the fact that Golomb et al. worked with larger nozzle diameters. The results of Milne et al. [2] do not lend themselves to the determination of the pressure dependence, directly. However, if we compare our relative intensities at room temperature and high pressures with data of Fig. 5 from ref. 2a, good agreement is found within a factor 1.2 for the dimer-ion signal.

The pressure and temperature dependence found by Yealland et al. [3] for the argon dimer concentration is derived from relatively high stagnation pressures and does not agree with our findings in the onset region; for $P_0 < P_L$, see Fig. 1. The scaling laws of Hagena [6] predict a value of $\alpha_2\beta_2 - \alpha_1\beta_1 \simeq 2.3$; we find the value 2.9±.3 for this quantity.

The total attenuation of the signal on each ion mass was measured. For a $1/e$ attenuation of the monomer beam by argon at 80 K, an Ar pressure of about $10^{-4}$ torr is needed over an experimental scattering length of 5 cm.

The angular resolution is estimated by the method of v. Busch [7] to amount to a 2 % (4 %) correction for the monomer (dimer) cross-section at $T_0 = 300$ K, assuming the total cross section to be 400 Å$^2$ (560 Å$^2$).

The attenuated intensity for mass $m$, $I_m$, depends on the pressure of the scattering chamber as $I_m = I_{m,0} \exp(-\sigma_m \cdot p_{\text{s.c.}} \text{ const})$. Therefore, we define a log attenuation $La$ (being proportional to the effective total collision cross-section $\sigma_m$) as $La = -(10^{-5}/p_{\text{s.c.}}) \log I_m/I_{m,0}$, where $p_{\text{s.c.}}$ is measured in torr.

In Fig. 2 the results for $T_0 = 173$ K are presented; the results for other $T_0$ are very similar. The $La$ for mass 40 is independent of $P_0$ below 1500 torr. For $T_0 = 294$, 223 and 123 K the stagnation pressures below which the $La$ for the monomer is constant are 6000, 3000 and 700 torr, respectively. The values of $La$ for different $T_0$ are corrected for the velocity spread in the scattering chamber (using formulas of Bernstein [8]) and for the finite angular resolution. [7]. The total cross-section thus found varies approximately with $v_{\text{rel}}^{-2/5}$, the velocity dependence for an $r^{-6}$ interaction potential. For the relative velocity, the value

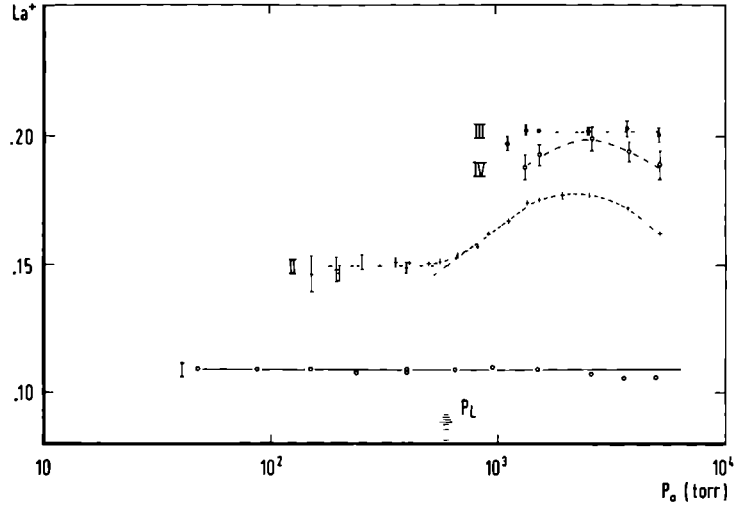


Fig. 2. Log attenuations vs. stagnation pressure $P_0$, at the stagnation temperature $T_0 = 173$ K. The log attenuation $La_n$ is proportional to the effective collision cross-section of neutral $Ar_n$ with Ar in the scattering chamber. The quantity $La^+$ is related to these log attenuations; it is the measured log attenuation for the $Ar^+$ (I), $Ar_2^+$ (II), $Ar_3^+$ (III), and $Ar_4^+$ signal (IV). For a unique correspondence between an ion signal and a specific neutral cluster $Ar_n$, the $La^+$ equals $La_n$ and is, thus, independent of $P_0$. Above the stagnation pressure $P_L$, this unique correspondence is lost for the $Ar_2^+$ signal.

belonging to full isentropic expansion [9] is taken. Glory undulations are unobserved; they are calculated to be small and completely averaged by the large spread of the relative velocity.

For $T_0 = 173$ K and pressure $P_0$ higher than 1500 torr the *La* yields lower values for the monomers. This can be caused by the increase in velocity of the beam [1b] and the deterioration of the angular resolution resulting from the larger effective source diameter [5]. Both effects have been discussed above.

For the dimer signal at mass 80 with $T_0 = 173$ K the *La* is constant within the experimental accuracy for stagnation pressure $P_0$ below $P_L = 600$ torr, see Fig. 2. Corresponding pressures $P_L$ are 1800, 1000 and 300 torr for 294, 223 and 123 K, respectively. At higher pressures the *La* rises and goes through a maximum. When these pressures $P_L$ are multiplied by $(294/T_0)^{\beta 2}$ (the value for $\beta_2$ obtained from our intensity measurements, as shown in Table 1, is used) an unique value $\tilde{P}_L$ is found, indicated by the arrow in Fig. 1. In our opinion, $\tilde{P}_L$ marks the relatively sudden appearance of larger clusters. For all $T_0$, larger clusters show up at the same dimer intensity.

Since the *La* is constant for $P_0 < P_L$ and no ion signals of larger clusters can be detected there (see Fig. 1) and since we find the correct pressure dependence ($\alpha_1 = 1.1 \pm 0.1$ and $\alpha_2 = 2.15 \pm 0.1$) we attribute the ion signal at mass 80 to the ionization product of neutral $Ar_2$ for $P_0 < P_L$. The constant value of *La* corresponds to the total effective dimer collision cross-section, averaged over all vibrational and rotational states. After correction for the finite angular resolution of our apparatus the total collision cross-section for the $Ar_2$–Ar system is found to be a factor $1.40 \pm 0.05$ larger than for the Ar–Ar system, independent of $T_0$. This means that the $C_6$-factor of the intermolecular potential is roughly twice as large for the dimer as for the monomer.

The rise of *La* for $P_0 > P_L$ is attributed to admixture of heavier polymers which in general will have larger cross-sections and will contribute to the signal at $m/e = 80$ by dissociative ionization. A signal of the larger cluster ions is detected at a pressure slightly above $P_L$ (see Fig. 1).

The levelling off of the *La* at $m/e = 80$ is attributed to scattering and break-up of beam clusters by the background in the source chamber.

For larger clusters, *La*-results are also given in Fig. 2; for $m/e = 120$ the *La*-values are independent of $P_0$, for $m/e = 160$ they are slightly smaller and vary somewhat with $P_0$. Under the (very questionable) assumption that the $m/e = 120$ signal does correspond to the trimer and the $m/e = 160$ signal to the quadrumer, we have estimated the relative total collision cross-section from the measured *La*. The same value is found for trimers and quadrumers, after applying the angular resolution correction, (about 6 % and 8 %) to the *La* [7].

It seems more realistic to abolish the idea of a simple correspondence between neutral trimers and quadrumers and the $Ar_3^+$ and $Ar_4^+$ signals and to face the possibility that the signals at $m/e = 120$ and 160 are for a large part due

to fragments of larger clusters. This possibility accords with the model that in supersonic nozzle beams at low $P_0$ only monomers and dimers are present, and that larger polymers (which suffer large dissociation at ionization) show up suddenly when a critical pressure is exceeded. The experimental pressure dependence of the trimer- and quadrumer-ion signal is the same, $\alpha_3 = \alpha_4 = 5.5 \pm 0.5$. (If the polymers could be produced under equilibrium conditions in the source, $\alpha_3 = 3$ and $\alpha_4 = 4$ would be expected.) The large exponents are at least compatible with the supposition that the ion signals at $m/e = 120$ and 160 originate, for a large part, from dissociative ionization. Let us assume, then, that the signals at $m/e = 120$ and 160 are due to a representative neutral parent of mass $m$, with an intensity $I_m$ and an effective $La_m$ equal to the measured average $La$ at $m/e = 120$ and 160 (see Fig. 2, where the log attenuations are shown for a scattering pressure of $10^{-5}$ torr; in the actual experiment about $3.4 \cdot 10^{-5}$ torr was used).

With this assumption we are able to estimate the ratio of detection probabilities $q_{m,3}/q_{m,2}$. Here, $q_{m,i}$ includes the probability of dissociative ionization of the neutral $Ar_m$ cluster resulting in the ion cluster $Ar_i^+$ as well as the transmission of the mass spectrometer and the multiplier efficiency for this ion. One has

$$I^+_{2,0} = q_{2,2} I_{2,0} + q_{m,2} I_{m,0} \tag{1}$$

$$I^+_{3,0} = q_{m,3} I_{m,0} \tag{2}$$

and

$$I^+_{2,0} \exp(-3.4 La^+_2) = q_{2,2} I_{2,0} \exp(-3.4 La_2) + q_{m,2} I_{m,0} \exp(-3.4 La_m) \tag{3}$$

The log attenuation $La_i^+$ is proportional to the effective cross-section, measured for the ion signal on mass $i$ as shown in Fig. 2.

From eqns. (1) and (2), it follows that

$$\frac{q_{m,3}}{q_{m,2}} \cdot \left[\frac{q_{m,2} I_{m,0}}{q_{2,2} I_{2,0}}\right] = \frac{I^+_{3,0}}{I^+_{2,0}} \left(1 + \left[\frac{q_{m,2} I_{m,0}}{q_{2,2} I_{2,0}}\right]\right) \tag{4}$$

The ratio $I^+_{3,0}/I^+_{2,0}$ is experimentally determined, see Fig. 1. The quantity

$$\left[\frac{q_{m,2} I_{m,0}}{q_{2,2} I_{2,0}}\right]$$

is related to the observed attenuations by

$$\left[\frac{q_{m,2} I_{m,0}}{q_{2,2} I_{2,0}}\right] = \frac{\exp(-3.4 La_2) - \exp(-3.4 La^+_2)}{\exp(-3.4 La^+_2) - \exp(-3.4 La_m)} \tag{5}$$

If we now use for $T_0 = 173$ K the values $La_2 = 0.150 \pm 0.003$, $La_m = 0.195 \pm 0.005$ and $La^+_2 = 0.157 \pm 0.002$ at $P_0 = 800$ torr or $La^+_2 = 0.164 \pm 0.002$ at $P_0 = 1000$ torr (see Fig. 2), we obtain values for $q_{m,2}/q_{m,3}$ between 10 and 20. Thus, we find a high relative probability to detect a neutral cluster of mass $m$ as an $Ar_2^+$ ion.

For the other values of $T_0$ the ratio $q_{m,2}/q_{m,3}$ is found between the same limits.

From eqn (5) it is found, from the given values of $La_2$, $La_m$ and $La_2^+$ that $q_{m,2}I_{m,0}/q_{2,2}I_{2,0}$ equals 0.2 at 800 torr and 0.5 at 1000 torr. This result indicates a strong admixture from large neutral clusters to the dimer signal, already at pressures slightly above $P_L$. Most of the measurements of Milne et al. [2] were done at stagnation pressures higher than $P_L$, therefore, the conclusions on rate constants of dimer formation should be taken with reserve To perform measurements below $P_L$ one really needs a very sensitive detector, otherwise the dimer ion signal is buried in noise (see the limited pressure range of constant attenuation in Fig. 2).

In a forthcoming paper we shall show that our experimental dimer results are in agreement with thermodynamic equilibrium predictions, based upon the assumption that the dimers are "prefabricated" in the source.

REFERENCES


1 (a) D Golomb, R E Good and R F Brown, *J Chem Phys*, 52 (1970) 1545, (b) D Golomb, R E Good, A B Bailey, M R Busby and R Dawbarn, *J Chem Phys*, 57 (1972) 3844
2 (a) T A Milne and F T Greene, *J Chem Phys*, 47 (1967) 4095, (b) T A Milne, A E. Vandergrift and F T Greene, *J Chem Phys*, 52 (1970) 1552
3 R M Yealland, J M Deckers, I D Scott and C T Tuori, *Can J Phys*, 50 (1972) 2464
4 A van Deursen and J Reuss, *Int J. Mass Spectrom Ion Phys*, 11 (1973) 483
5 A H M Habets, H C W Beijerinck and N F Verster, *Proc Symp Rarefied Gas Dyn, 9th*, 1974
6 O F Hagena, *Entropie*, 42 (1971) 42
7 F V Busch, *Z Phys*, 193 (1966) 412
8 R B Bernstein, *Comments At Mol Phys*, 4 (1973) 43
9 J B Anderson and J B Fenn, *Phys Fluids*, 8 (1965) 780.

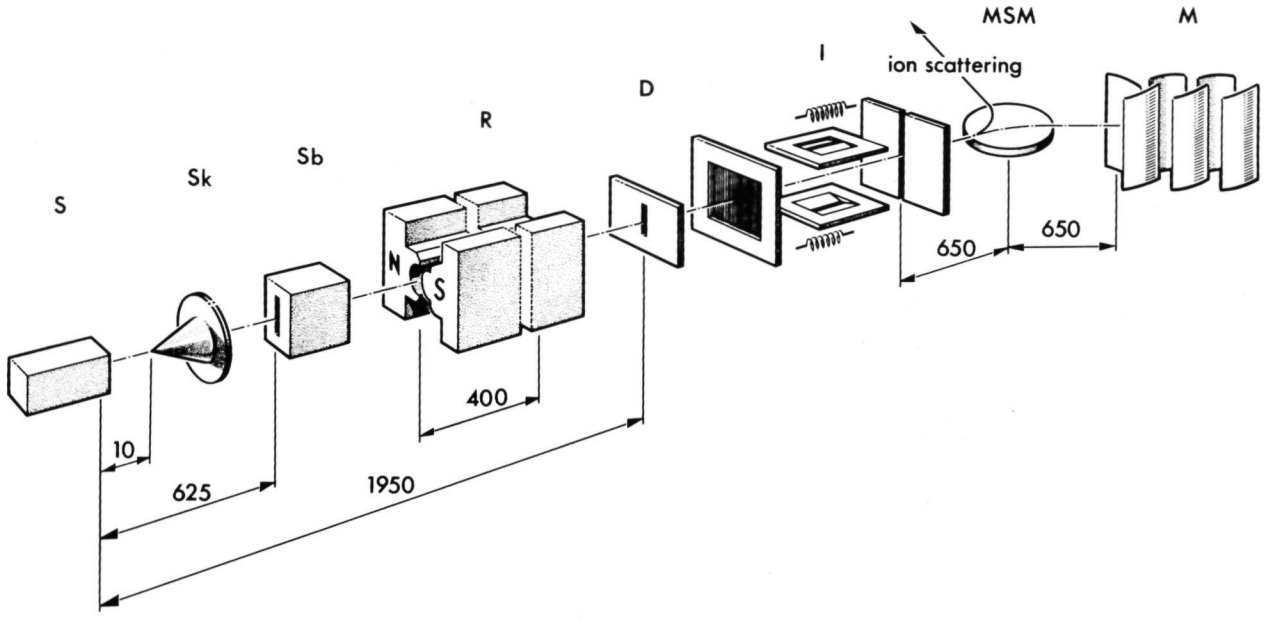


*Fig. IV.1. Schematic view of the apparatus.*
The cluster beam is formed by the expansion of gas from the nozzle source S and by the conical skimmer Sk; it passes through the scatterbox Sb and the Rabi type magnet R. The beam is collimated by a slit of the scatterbox and the detectorslit D. After D the cluster beam enters the ionizer I; the ions are mass selected in magnet MSM and amplified by electron multiplier M. Reversing the magnetic field in MSM the ions can be used for further experiments ("ion scattering"). All distances given are in mm.

# IV INTENSITIES AND CROSS SECTIONS OF Ne, $H_2$, $N_2$, NO AND $O_2$ CLUSTERS IN A MOLECULAR BEAM

## IV 1 INTRODUCTION

Persuing our earlier effort (ref 1), we have investigated molecular beams of Ne, $H_2$, $N_2$, NO, and $O_2$ clusters The temperature and pressure dependence of the ion signals have been measured for masses up to three times the monomer mass

The neutral beam is attenuated by argon- or helium-gas in a scatterbox While the total collision cross section itself is of interest, it serves at the same time to check what neutral parent belongs to a certain ion mass (ref 1) Only for monomers and dimers we were able to determine a "clean" cross section

For Ar we have been able to plot the intensities vs reduced source pressures $P_{red}$, such that for all source temperatures $T_0$, a single curve is obtained for each ion mass The aim of this investigation is to test whether a similar reduction is also possible for another noble gas, Ne, for a nearly noble gas, $H_2$, and also for diatomic molecules, $N_2$ and NO

For $H_2$ and the paramagnetic gases NO and $O_2$, the magnetic properties of the dimer have been compared with those of the monomers, using a Rabi type deflection magnet of 40 cm length and a maximum field gradient of 20 kGauss $cm^{-1}$

In addition to the insertion of this deflection magnet, the original set-up described in ref 1 has been changed by replacing the small mass spectrometer magnet by a more powerful one (a switching magnet, model 1038, Spectromagnetic Industries, 14 cm pole diameter) At 900 eV ion energy the mass range extends up to 2500 amu

All measurements have been done using a 26 μ nozzle diameter The distance between source and scatterbox amounts to 65 cm, that between the source and detector slit to 195 cm Good collimation of the beam is ensured by the rectangular opening of the scatterbox, 0 4x12 $mm^2$, and the slit in front of the detector, 0 8 x 8 $mm^2$ Extra collimation at the source was tried but never felt necessary A view of the apparatus is given in fig IV 1

## IV 2 THE INTENSITIES

In fig IV 2a the intensities are drawn as a function of the reduced pressure for the isotopes of the Ne-monomer and for their dimers The Ne-gas used has the natural composition, 90 92% $^{20}Ne$, 8 82% $^{22}Ne$, 0,257% $^{21}Ne$ The figure shows the $^{20}Ne$ monomer intensity divided by a factor 10, in consequence it coincides with the $^{22}Ne$ monomer, the omitted signal of the other isotope scales according to its natural abundance

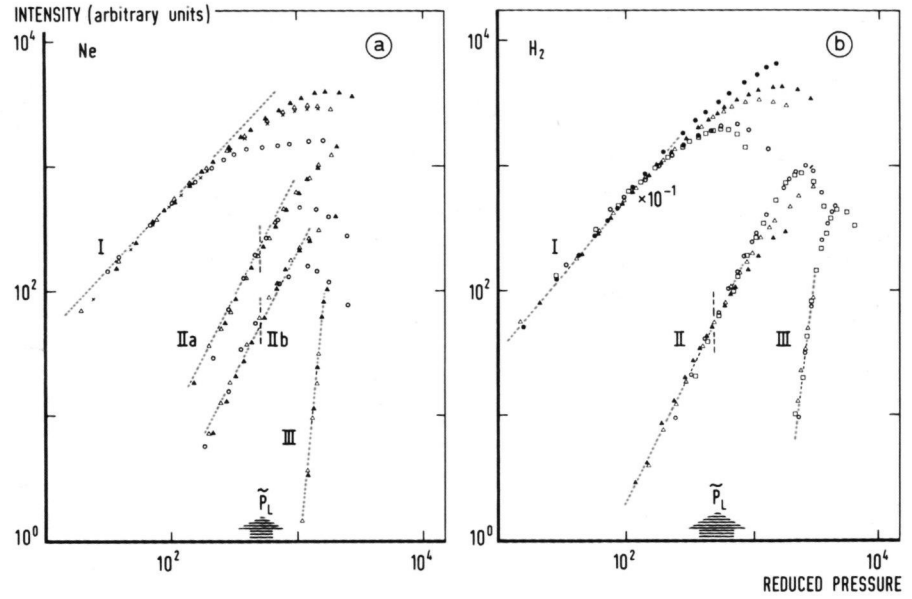


*Fig. IV.2. Intensity vs. reduced pressure* for Ne (a) and $H_2$ *(b)*. In the left part of the figure the symbol I corresponds to the $^{20}Ne^+$ intensity divided by a factor 10; the $^{22}Ne^+$ intensity at $T_0$= 65K is indicated by x. The symbol IIa corresponds to $^{20}Ne_2^+$, IIb to $^{20}Ne^{22}Ne^+$, and III to $^{20}Ne_3^+$. In the right part of the figure the symbol I belongs to $H_2^+$, II to $H_3^+$ and III to $H_5^+$. The monomer intensity (I) is displayed divided by a factor 10. The intensities are measured at temperatures $T_0$ = 100K (▲), $T_0$ = 65 K (Δ ,x), and $T_0$ = 33 K (O). For $H_2$ we have added the intensities for $T_0$ = 273K (●, monomer only) and $T_0$ = 28 K (□).
The abscissa represents the true pressure $P_0$ in torr for $T_0$ = 65 K.
At other temperatures reduction factors $P_0/P_{red}$ are applied for each ion mass, see table IV.I. At the reduced pressure $\tilde{P}_L$ the dimer signal becomes contaminated by fragments of larger clusters.

For a source temperature $T_0$=65K the reduced pressure $P_{red}$ equals the true source pressure $P_0$; for other temperatures the reduction factors are given in table IV.1.

No scaling other than for the monomer ion isotopes is applied in vertical direction. At higher pressures the intensity curves start to diverge, the high temperature ones always above the low temperature ones. This behaviour stems from the fact that at lower source temperatures the production of heavier clusters takes place at lower reduced pressures, causing a decrease of intensity. Also, heavier clusters start to appear; $Ne_5^+$ ions are observed but not shown in fig. IV.2.

The dimer ion isotopes have a constant ratio of intensities, $I_{40}/I_{42} \simeq 4$, as expected from statistical considerations.

In fig. IV.2b the results for $H_2$ are given. As discussed in ref. 2 we have observed ions $H_2^+$, $H_3^+$ and $H_5^+$; also higher masses were detected (ref. 2), but

are not considered in the present work. For the reduction factors $P_0/P_{red}$ see table IV.1.

For the monomer ion signals the diverging tendency at high pressures is similar to that observed for Ne and Ar (ref. 1). However, for the $H_3^+$– ion the sequence is reversed. In our interpretation the reversal is caused by significant fragmentation of heavy clusters into $H_3^+$-ions in the ionizer.

In fig. IV.3a and 3b the intensities are given for $N_2$ and NO, respectively, for temperatures $T_0$ between 130 K and 300 K. In table IV.1 the reduction factors $P_0/P_{red}$ are given. Signals of heavier clusters have been observed, for instance up to $N_{14}^+$, but are not displayed in fig. IV.3. Contrary to the case of $H_2$, here the ions of even mass have intensities stronger than those of odd mass. For instance, fourty times the $N_3^+$-signal is observed on $N_4^+$, whereas fifty times the $H_6^+$-signals equals roughly the $H_5^+$–signal (ref. 2).

The pressure range where we can draw a straight line through the results in fig. IV.2 and 3 is called the onset region. The cross section results of the following section show that in this region the monomer (dimer) ion signals originate from neutral monomers (dimers).

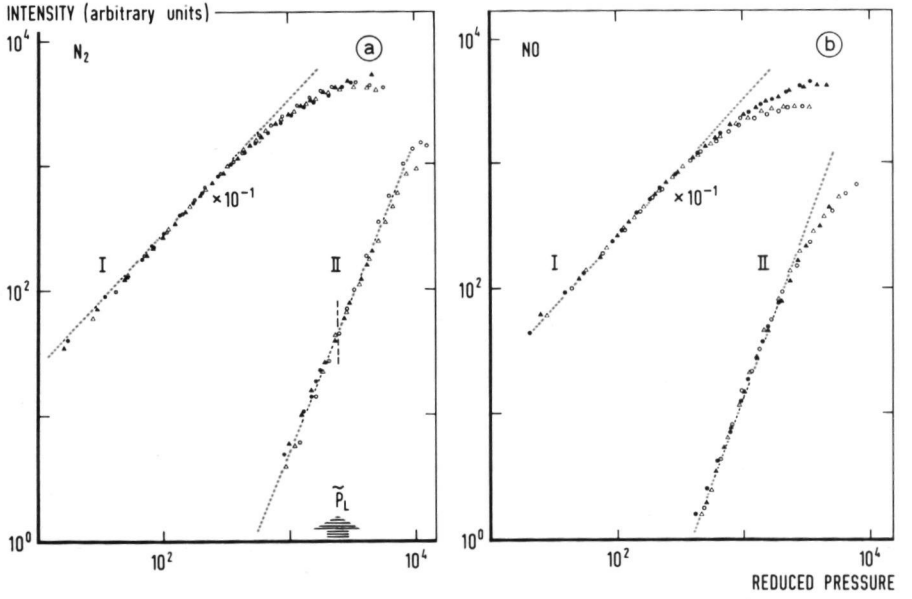


caption to fig IV.3

*Fig. IV.3. Intensities vs. reduced pressure* for $N_2$ (a) and NO (b).
The intensities are measured at source temperatures $T_0$ = 296 K (●), $T_0$ = 223 K (▲), $T_0$ = 173 K (△), and $T_0$ = 133 K (O). The abscissa represents the true pressure $P_0$ in torr for $T_0$ = 233 K. At other temperatures reduction factors $P_0/P_{red}$ have been applied, see table IV.I. The monomer ion signal (I) is displayed, divided by a factor 10; The dimer ion signals $N_4^+$ and $(NO)_2^+$ are indicated by II. For $N_2$ the reduced value $\tilde{P}_L$ is indicated; no $P_L$ can be defined for NO.

TABLE IV.1

| | m | 28 | 33 | 65 | 100 | 296 | (K) |
|---|---|---|---|---|---|---|---|
| $Ne^+$ | 1 | — | .48 ± .03 | 1 | 1.7 ± .1 | — | |
| $Ne_2^+$ | 2 | — | .24 ± .02 | 1 | 2.0 ± .1 | — | |
| $H_2^+$ | 1 | .44 ± .02 | .52 ± .03 | 1 | 1.30 ± .05 | 3.5 ± .2 | |
| $H_3^+$ | 2 | .16 ± .01 | .23 ± .01 | 1 | 2.1 ± .1 | — | |
| $H_5^+$ | 3 | .11 | .16 | 1 | — | — | |

| | m | 133 | 173 | 223 | 296 | (K) |
|---|---|---|---|---|---|---|
| $N_2^+$ | 1 | .65 ± .05 | .88 ± .05 | 1 | 1.4 ± .1 | |
| $N_4^+$ | 2 | .25 ± .02 | .53 ± .05 | 1 | 2.5 ± .2 | |
| $NO^+$ | 1 | .63 ± .03 | .90 ± .05 | 1 | 1.32 ± .1 | |
| $(NO)_2^+$ | 2 | .31 ± .02 | .55 ± .05 | 1 | 2.4 ± .1 | |

*Table IV.1. Reduction factors* $f = P_0/P_{red}$, $I^+_{m,0} \sim P_0^{\alpha_m} / T_0^{\alpha_m \beta_m}$

TABLE IV.2

| gas | $\alpha_1$ | $\beta_1$ | $\alpha_2$ | $\beta_2$ | $\alpha_3$ | $\beta_3$ |
|---|---|---|---|---|---|---|
| Ne | 1.1 ± .1 | 1.1 ± .1 | 2.0 ± .1 | 1.9 ± .1 | — | — |
| $H_2$ | 1.1 ± .1 | .9 ± .1 | 2.0 ± .1 | 2.0 ± .1 | 7.8 ± .5 | 2.7 ± .1 |
| $N_2$ | 1.1 ± .1 | .9 ± .1 | 2.5 ± .2 | 2.85 ± .1 | — | — |
| NO | 1.1 ± .1 | .9 ± .1 | 2.8 ± .1 | 2.5 ± .1 | — | — |

*Table IV.2. Exponents* $\alpha_m$ *and* $\beta_m$ *for the intensities in the onset region.*

In the onset region the measured intensities $I^+_{m,0}$ are approximately proportional to $P_0^{\alpha_m} / T_0^{\alpha_m \beta_m}$, m = 1 for the $Ne^+$, $H_2^+$, $N_2^+$ and $NO^+$ signals, m = 2 for the $Ne_2^+$, $H_3^+$, $N_4^+$ and $(NO)_2^+$ signals. Values for $\alpha_m$ and $\beta_m$ are shown in table IV.2.

The pressure dependence of $I^+_{m,0}$ is in accordance with expectation, $\alpha_1 \simeq 1$. For $I^+_{2,0}$ one expects a proportionality with the squared density of the monomer in the source.

Experimentally we find $\alpha_2 = 2.0 \pm 0.1$ for Ne, Ar (ref.1) and $H_2$; for $N_2$, NO and $O_2$, however, we find $\alpha_2 = 2.5 \pm .2$, 2.8 ± .1 and 2.7 ±.2, respectively.

Even a simple equilibrium theory for dimer concentration predicts a much more complicated temperature dependence than the proportionality with $T_0^{\alpha_2 \beta_2}$. However, for the limited temperature range investigated this approximation gives the right reduction factor $P_0/P_{red}$ within 7% for Ne and $H_2$, within 6% for $N_2$ and within 9% for NO.

With respect to ref. 1 the scattering technique has been improved attaching an ionization gauge directly to the 80 K scatterbox (see also ref.3). The filament of the gauge is mounted under tension to prevent geometrical changes during operation. Thereby, the reproducibility is kept within 1% per day. During long measuring periods the gauge is not swiched off for weeks. To attenuate the neutral beam a pressure of about $10^{-4}$ torr is maintained in the scatterbox; for the unattenuated beam the box is pumped down to about $2.x10^{-7}$ torr.

In fig. IV.4a and 4b the total collision cross section results for Ne and $H_2$ are displayed with a light and a heavy scattering partner, respectively. As in ref.1 we are able to define a pressure limit $\tilde{P}_L$, below which the dimer ion signal corresponds to a neutral dimer parent. The range for $\tilde{P}_L$ indicated in fig. IV.2, 3, 4 and 5 is obtained by dividing the $P_L$ values by the reduction factors for the dimer intensities (see table IV.1) A general criterion will be discussed in the next section.

The velocity of the beam molecules, $v_1$, has been calculated from the source temperature $T_0$ assuming full isentropic expansion, $v_1 = (2C_p T_0)^{\frac{1}{2}}$; $C_p$ is the specific heat at constant pressure per unit mass. The average relative

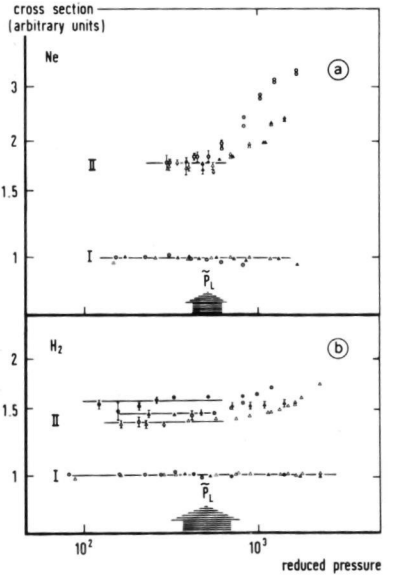


*Fig. IV.4. Apparent cross section vs. reduced pressure* for Ne (a) and $H_2$ (b) of monomers (I) and dimers (II).
The different symbols correspond to different temperatures, $T_0$ = 100 K (▲), $T_0$ = 65 K (Δ); for Ne the results at $T_0$ = 33 K (O), for $H_2$ those at $T_0$ = 166 K (●) and $T_0$ = 30 K (O) are added. As target molecule He is used for Ne, and Ar for $H_2$. The ordinates are logarithmic; at all values of $T_0$ the avarage value of $\sigma_1$ is taken equal to unity for both Ne and $H_2$. The abscissa represents the true pressure $P_0$ for $T_0$ = 65 K; at other temperatures reduction factors have been applied, see table IV.1. For $T_0$ = 166 K interpolated reduction factors are used. For $P_{red} \leq \tilde{P}_L$ the dimer cross section is determined. The results for both Ne isotopes are shown together. The dimer measurements for Ne do not extend to very low pressures because of detector noise due to residual background ions. For Ne no variation in $\sigma_2/\sigma_1$ is found, for $H_2$ a slight variation with $T_0$ is apparent. The shaded regions for $\tilde{P}_L$ are obtained by a reduction of $P_L$ with the same factors as for the dimer intensities, see table IV.1.

velocity v for different scattering partners has been calculated from $v_1$ and the thermal velocity of the scatter gas, $\alpha_s$ ; $v = (v_1^2 + \alpha_s^2)^{\frac{1}{2}}$ . Fig. IV.4 shows that the velocity dependence of $\sigma_2/\sigma_1$, the ratio of dimer and monomer cross section, is small or negligible. For this reason we refrained from a more accurate velocity determination.

In fig. IV.5a and b similar results are given for $N_2$ and NO. No velocity dependence of $\sigma_2/\sigma_1$ is detected. With a heavy scattering partner, the value of $\sigma_2/\sigma_1$ equals 1.34 ± .02 for NO, 1.40 ± .03 for $N_2$, and 1.40± .02 for $O_2$. The ratio found for Ar (cf. ref. 1) is $\sigma_2/\sigma_1 = 1.39 \pm .02$, for Ne $\sigma_2/\sigma_1 = 1.35 \pm .05$. For $H_2$ the values range from $\sigma_2/\sigma_1 = 1.36 \pm .02$, at $v_1 \simeq 1200$ msec$^{-1}$, to $\sigma_2/\sigma_1 = 1.55 \pm .04$, at $v_1 \simeq 1900$msec$^{-1}$.

For the light scattering partner (He) larger $\sigma_2/\sigma_1$ ratios are found, generally; $\sigma_2/\sigma_1 = 1.64 \pm .02$ for $N_2$, $\sigma_2/\sigma_1 = 1.57 \pm .05$ for $O_2$; $\sigma_2/\sigma_1 = 1.77 \pm .02$ for Ne and $\sigma_2/\sigma_1 = 1.96 \pm .06$ for $H_2$. For the molecular system NO the ratio $\sigma_2/\sigma_1$ is found slightly smaller, $\sigma_2/\sigma_1 = 1.51 \pm .02$.

The angular resolution correction is applied to $\sigma_2/\sigma_1$ following ref. 4. For the heavy scattering partner, where the interaction is dominated by a $r^{-6}$–attraction, this correction equals roughly the experimental uncertainty. The relative correction due to the spread in relative velocity is the same for $\sigma_2$ and $\sigma_1$ (ref. 5.). The light collision partner poses the problem that the angular resolution correction according to ref. 4 becomes rather inaccurate for two reasons. Firstly, the velocity dependence is not in agreement with a pure $r^{-6}$–potential. Secondly, the velocity of the target molecules is comparable to $v_1$; in this case the formulas of ref. 4 are not properly valid. Lack of a better procedure has forced us neverthe-

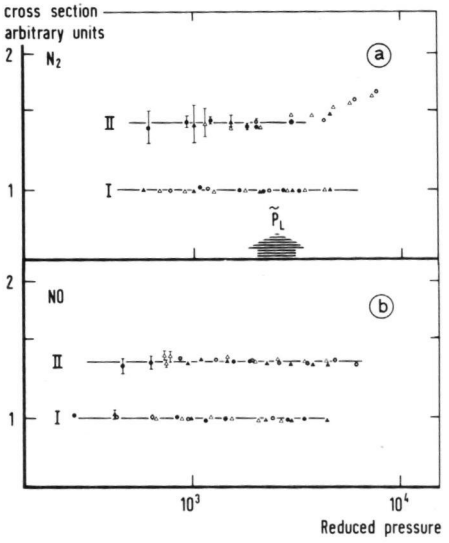


*Fig. IV.5. Apparent cross section vs. reduced velocity* for $N_2$ (a) and NO (b) of monomers (I) and dimers (II).
The different symbols correspond to different temperatures, $T_0$ = 296 K (●), $T_0$ = 223 K (▲), $T_0$ = 173 K (Δ), and $T_0$ = 133 K (O). The abscissa represents the true pressure $P_0$ in torr for $T_0$ = 233 K; for other temperatures a reduction is applied equal to that for the intensities (table IV.1). For both $N_2$ and NO, Ar is used as target gas. For all temperatures $\sigma_1$ is independent of the source pressure and is taken equal to unity. For $N_2$ a pressure $\tilde{P}_L$ is defined; from reduced pressures $P_{red} \leq \tilde{P}_L$ the dimer cross section $\sigma_2$ is determined. For NO the cross section $\sigma_2$ is constant up to the highest pressures, where ion signals of larger clusters are already present. Both for $N_2$ and NO, the ratio $\sigma_2/\sigma_1$ is equal for all $T_0$.

less, to use the correction method of ref. 4. The statistical error given for $\sigma_2/\sigma_1$ does not include the uncertainty of this correction

The discussion of the ratio $\sigma_2/\sigma_1$ for a heavy scattering partner can be based on the expression for the total collision cross section (ref. 6)

$$\sigma_{tot} = 8\,083(C_6/\hbar v)^{2/5} \qquad \text{(IV 1)}$$

From eq. IV.1 follows $C_{6\,d}/C_{6\,m} = (\sigma_2/\sigma_1)^{2/5}$. Consequently, $\sigma_2/\sigma_1 = 1\,32$ yields $C_{6\,d} = 2C_{6\,m}$ (ref. 1). Observed ratios 1 34 - 1 45 correspond to $C_{6\,d}/C_{6\,m}$ between 2.0 and 2.5 This ratio appears reasonable to us; theoretical predictions for $C_{6\,d}/C_{6\,m}$ do not exist at this moment.

For $H_2$-Ar scattering and wherever He is used as scattering partner, glories in the total collision cross section might have been expected. However, due to the velocity averaging for He (average velocity in the 80K scatterbox 600 $msec^{-1}$) the glories are smoothed out entirely. With the $H_2$– beam this averaging effect is much smaller because here the heavy and slow partner is in the scatterbox. Here, $\sigma_2/\sigma_1$ is found to vary slightly over the large velocity range, $v_1$ between 800 and 1850 $msec^{-1}$.

If one neglects all possible inelastical events (rotational excitation and dissociation of the loosely bound $(H_2)_2$-complex), one can calculate $\sigma_2/\sigma_1$ under simplifying assumptions concerning the interaction potential. In fig. IV.6 results of such a calculation are shown.

The monomer cross section is calculated (ref.7) for the Lennard Jones potential with $\varepsilon$ and $R_m$ taken from ref. 3 Our measured monomer cross section $\sigma_1$ (fitted to the calculated value at 1180 m $sec^{-1}$) agrees with the calculations to within the experimental error The spread in relative velocity due to the thermal velocity of the target gas is indicated by the horizontal bars on $\sigma_1$.

In fig. IV.6. the experimental points of $\sigma_2$ are derived from the calculated $\sigma_1$ and the measured ratios $\sigma_2/\sigma_1$.
We calculated (ref. 7) a dimer cross section for various sets of Lennard Jones parameters. A reasonable fit is shown in fig. IV.6, for $C_{6\,d} = 2.5C_{6\,m}$ (IIa) and $2.7\,C_{6\,m}$ (IIb); the product $\varepsilon R_m$ is kept constant and taken equal to the monomer value because this guarantees the absence of glory undulation in $\sigma_2/\sigma_1$.
The $C_{6\,d}/C_{6\,m}$ value obtained are similar to the results for the heavier systems.

## IV 4 THE MAXIMUM PRESSURE $P_1$ FOR PURE DIMER BEAMS

One main result of this work is the firm establishment of experimental conditions under which the dimer ion signal corresponds to pure dimers, with negligible contamination from fragments of heavier clusters. For each source

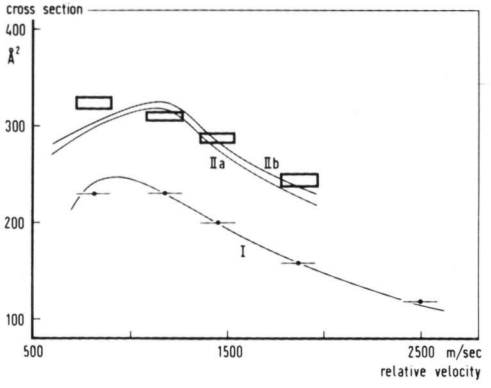


*Fig. IV.6. Calculated and measured cross section $\sigma_2$ and $\sigma_1$ vs. velocity* for $H_2$-Ar.
The curve indicated by (I) represents the calculated monomer cross section. The measured cross section $\sigma_1$ is put equal to the calculated cross section at v = 1180 m/sec. The monomer cross section at v = 1460, 810 and 760 m/sec follow from this choice and are then equal to the calculated ones within their errors. The dimer cross sections are obtained from the measured ratios $\sigma_2/\sigma_1$. The curves IIa and IIb are calculated for $C_{6,d}$ =2.7 $C_{6,m}$ and 2.5 $C_{6,m}$ respectively, with $C_{6,m}$ = $2.80\times10^{-11}$ erg.Å$^6$; $\varepsilon R_m$ = $3.37\times10^{-14}$ erg.Å is taken equal for monomers and dimers.

temperature $T_0$ we find a limit pressure $P_L$ below which the simple correspondence prevails. The values of $P_L$ are collected in table IV.3. The limit pressure is of technical interest to those who want to design experiments. Therefore, we tried to condense our experience into a simple prescription using the intermolecular potential depth $\varepsilon$ and the minimum position $R_m$ as scaling parameters.

All our measurements on the noble gases Ar and Ne, and $H_2$ and $N_2$, performed with a $d_0$ = 26 μ nozzle diameter, lead to $P_L$-values given by the following equation (within a factor 1.3)

$$P_L = 0.6 \times \varepsilon R m^{-3} . \{kT/\varepsilon\}^{(2-3\varkappa)/(2-2\varkappa)} . (R_m/d)^{.55} \qquad \text{(IV.2)}$$

Eq. IV.2 is not in contradiction with the general formulas given in ref. 8; actually, the temperature dependence correponds with the lower limit of Hagena and Obert. The temperature dependence for Ar and $N_2$ agrees, too, with the temperature dependence observed by Golomb et al. (ref. 9) for the pressure corresponding to the maximum of the dimer ion signal. At this pressure large clusters are abundantly present in the beam. Its value is about three times higher than the value of $P_L$, as can be seen from fig. III.1, or calculated from the experimental result and the scaling laws of ref. 9.

Eq. IV.2 is tested for $d = d_0 = 26\,\mu$, only. The last factor is added in view of the evidence (ref. 9) that beam condensation is determined by the product $P_0.d^{.55}$, at fixed source temperature. The scaling of the nozzle diameter d with $R_m$ is in accordance with the principle of corresponding jets (ref. 8).

table IV.3

| | | | | |
|---|---|---|---|---|
| $T_0$ | 33 | 65 | 100 | |
| Ne | 100 | 600 | 1100 | |
| $H_2$ | 90 | 600 | 1700 | |
| $T_0$ | 123 | 173 | 223 | 294 |
| Ar | 300 | 600 | 1000 | 1800 |
| $T_0$ | 133 | 173 | 223 | 294 |
| $N_2$ | 800 | 1100 | 3000 | – |

*Table IV.3. Values of* $P_1$ in torr at various $T_0$ for Ne, $H_2$, Ar, and $N_2$.

The dimer signal of NO forms an exception; here no contribution from fragmentation of larger clusters to the dimer ion signal is indicated by our measurements. At the maximum source pressure used many heavier clusters are present in the beam and the dimer ion signal levels off already.

## IV.5 MAGNETIC DEFLECTION

We have looked for information concerning the magnetic properties of dimers of $H_2$, NO and $O_2$ in the beam by measuring their deflection in an inhomogeneous magnetic field.

For a well collimated $H_2$-beam at 26 K source temperature ($v_1$ = 750 m/sec) the ortho-monomers in the $m_I = \pm 1$ state can be bent off the beam axis. We have varied the position of a slit (.1 mm width) in front of the Rabi magnet. For a broad $H_2$-beam the three $m_I$-states are clearly resolved; at three different slit positions distinct maxima of the signal are observed (see also ref. 10).

Without a magnetic field the dimer beam is sharply peaked, corresponding to good collimation of the beam. With magnetic field on, a broad distribution is measured by varying the slit position. The f.w.h.m. of the distribution is equal to the separation of the two $m_I = \pm 1$ states for the monomer. This indicates that the $H_2$-dimers in the beam have magnetic moments comparable to those of the

$H_2$-monomers. Consequently, the $H_2$-dimers can be investigated by magnetic resonance spectroscopy, a method described in detail by Ramsey (ref. 11). The total signal of pure dimers amounts to 1% of the monomer signal at maximum.

In the liquid phase, dimers of NO are known to be diamagnetic; also solid NO is found to consist of diamagnetic NO-dimers. On the other hand, the paramagnetism of $O_2$ is preserved in the liquid phase. However, from analysis of magnetic susceptibility it has been suggested that in $O_2$ at low temperatures some molecules form nonmagnetic dimers (ref. 13). Knobler (ref. 14) has sought evidence for these nonmagnetic dimers in the liquid.

We have investigated whether gaseous dimers of NO and $O_2$ posses magnetic moments. The decrease of the dimer intensity due to the inhomogeneous magnetic field is compared with that of the monomer intensity.

For NO-monomers a slow monotonuous decrease is observed to about 40% of the full beam at the highest field gradient obtained in our experimental set up, about 20 kGauss.cm$^{-1}$. At low magnetic field no sudden decrease has been found due to the deflection of the $\Pi_{3/2}$-state. This agrees with the experimental result (ref. 15) that in a nozzle expansion the electronic temperature (calculated from the relative population of the $\Pi_{1/2}$ and the $\Pi_{3/2}$ states) decreases similarly to the translational temperature. In the highly expanded jet of our experiment the $\Pi_{3/2}$ -state may be completely depopulated.

For NO dimers no decrease because of the magnetic deflection is detected. The absence of a magnetic moment can be explained in two ways. If paramagnetic $\Pi_{3/2}$ molecules are present in the beam, it is not likely that they will form stable dimers with other molecules. The energy of the electronic excitation exceeds the binding energy of the dimer. Because many degrees of freedom are coupled in a dimer, this energy can be transfered to rotation and vibration, causing dissociation. We are left with the diamagnetic dimers of two $\Pi_{1/2}$ molecules only. On the other hand, assuming that a dimer containing one or two $\Pi_{3/2}$ molecules has a lifetime long enough to reach the detector, its magnetic moment will be averaged to zero by the end over end rotation, in first order. For the end over end rotation large quantum numbers are allowed, see sect. VI.3.

The $O_2$-monomer signal drops to about 30% of its maximum value at low fields already, due to the deflection of the $^3\Sigma(m_\Sigma = \pm 1)$ states. At higher fields the signal approaches zero because the $^3\Sigma(m_\Sigma = 0)$ state is also deflected now, due to its small magnetic moment originating from the rotation of the molecule coupled to the electronic spin. We observe that $O_2$ dimers can be deflected, too; the maximum obtainable decrease of signal is about 70%. Therefore, $O_2$ dimers are paramagnetic. We consider the dispute about the appearence of diamagnetic $O_2$ dimers as settled (ref. 14). There are none.

Paramagnetic $O_2$ dimers will be interesting objects for a magnetic beam resonance study, although intensity problems may be severe. Admixture of He may improve the situation (see sect. VII.4).

1. A. v. Deursen, A. v. Lumig and J. Reuss, Int. J. Mass Spectrom. Ion Phys., *18* (1975) 129, ch. III of this thesis.
2. A. v. Deursen and J Reuss, Int J Mass Spectrom. Ion Phys., *11* (1973) 483, ch. II of this thesis.
3. R. Helbing, W. Gaide and H Pauly, Z. Physik, *208* (1968) 215.
4. F. v. Busch, Z Physik, *193* (1966) 412.
   F. v. Busch, H. J Strunck and Ch Schlier, Z Physik, *199* (1967) 518.
5. R B. Bernstein, Comments At. Mol. Phys., *4* (1973) 43.
6. L D. Landau and E. M. Lifshitz, "Quantum Mechanics", Pergamon Press, London (1959).
7. Calculations performed by L. Zandee, using a computer program of H. Moerkerken.
8. O. F. Hagena and W. Obert, J. Chem. Phys., *56* (1972) 1793.
9. D. Colomb, R. E Good, A. B. Bailey, M. R. Busby and R. Dawbarn, J. Chem. Phys., *57* (1972) 3844.
10. L. Nelissen, J. Reuss and A. Dynamus, Physica, *42* (1969) 619
11. N. F. Ramsey, "Molecular Beams", Oxford University Press, New York (1956).
12. H. Bizette and B Tsai, Compt. Rend., *204* (1937) 1638.
13. G. N. Lewis, J. Am. Chem. Soc., *46* (1924) 2027.
14. C. M. Knobler, Thesis, Leiden (1961).
15. S. Stolte, private communication.

# V EXPERIMENTAL INVESTIGATION OF SMALL He CLUSTERS

A. P. J. van Deursen and J. Reuss

*Katholieke Universiteit, Fysisch Laboratorium, Toernooiveld, The Netherlands*
(Received 16 December 1974; revised paper received 2 September 1975)

The question of the existence of a bound van der Waals complex for $He_2$ has received attention in the literature recently. Accurate scattering studies by Farrar and Lee[1] and by Bennewitz *et al.*[2] suggest the absence of a bound state for the $He_2$ system. The potentials obtained are in fair agreement with theoretical results by Bertoncini and Wahl[3] and by Schaefer *et al.*[4] However, as is discussed by Bennewitz,[2] a 1.4% increase in the potential depth suffices to accomodate one bound state with zero angular momentum.

In the course of measurements of the production of molecular clusters[5] we have searched for helium clusters. In our molecular beam machine we are able to cool the source to 6 K. The source pressure $P_0$ can be varied up to 6 atm for a nozzle diameter of 6 $\mu$. The beam is detected by a magnetic spectrometer.[5] The ionizer is adjusted to work without any detectable space charge.

The measured intensities of the ions $He_n^+$, $n = 1-4$ are given in Fig. 1(a) as a function of $P_0$, at $T_0 = 7$ K. $He_2^+$ ions are observed for values of $P_0$ larger than 200 torr. The intensity of $He^+$ increases linearly with $P_0$ for $P_0 < 400$ torr, and the intensity of $He_2^+$ varies with $P_0^3$ up to $p_0 = 800$ torr. Above 1100 torr the $He_3^+$ and $He_4^+$ ions appear; their intensity is roughly proportional to $P_0^{10}$. The heaviest ion detected at 1500 torr was $He_{13}^+$.

To determine the correspondence between cluster ions and the neutral parent clusters, a scattering chamber filled with argon gas at 80 K is placed in the neutral beam path. A similar experiment with argon clusters is described in Ref. 6. The effective total cross section for the different ion signals is given in Fig. 1b.

The cross section of the $He^+$ signal is constant over the entire pressure range. We conclude that the $He^+$ ions are due to the unclustered He atoms in the neutral beam.

The cross section of the $He^+$ signal is constant for inlet pressures up to 500 torr. In this pressure range one neutral parent cluster for the $He_2^+$ ion exists.

From three arguments we conclude that the $He_2^+$ ions originate from neutral $He_3$ clusters for $P_0$ between 200 and 500 torr, which dissociate to $He_2^+$ in the ionizer.

Firstly, the intensity is proportional to $P_0^3$. For the $He_2$ parents a proportionality of $P_0^2$ is expected.

Secondly, the ratio of the total cross sections for $He^+$ and $He_2^+$ is found to be as large as $1.95 \pm 0.1$. It is difficult to reconcile this large ratio with a $He_2$ parent.[6]

Finally, the intensity of the trimers relative to the

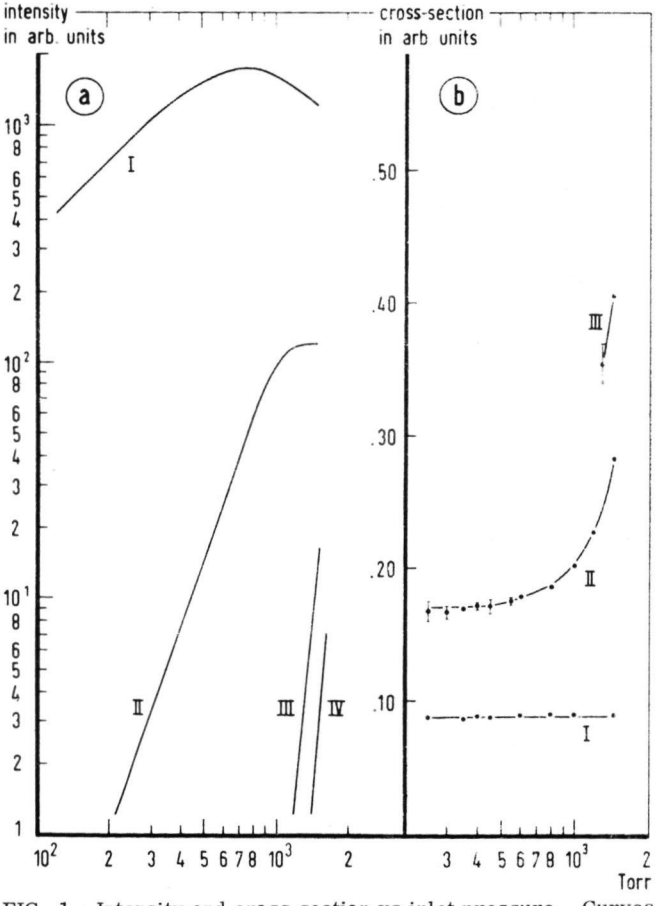


FIG. 1. Intensity and cross section vs inlet pressure. Curves I, II, III, and IV correspond to ion masses 4, 8, 12, and 16, respectively.

monomers can be estimated[6] assuming equilibrium in the source and assuming one bound state for a trimer. Good agreement is found with experimental values for a trimer parent; for a dimer parent, however, the estimated concentration is too large by an order of magnitude.

At pressures larger than 500 torr the cross section on $He_2^+$ rises owing to admixture of larger clusters in the beam and dissociative ionization. The $He_3^+$ cross section at $P_0 > 1000$ torr varies strongly with $P_0$ and is about 3.5 times larger than the He cross section. It seems impossible to link this behavior with a unique parent cluster.

In conclusion, our results agree with the prediction that there is no bound state for $He_2$.


[1]J. H. Farrar and Y. T. Lee, J. Chem. Phys. 56, 5801 (1972).
[2]H. G. Bennewitz, H. Busse, H. D. Dohman, D. E. Oates, and W. Schrader, Z. Physik 253, 435 (1972).
[3]P. Bertoncini and A. C. Wahl, Phys. Rev. Lett. 25, 991 (1970) and J. Chem. Phys. 58, 1259 (1973).
[4]H. F. Schaefer, D. R. McLaughlin, F. E. Harris, and B. J. Adler, Phys. Rev. Lett. 25, 988 (1970). D. R. McLaughlin and H. F. Schaefer, Chem. Phys. Lett. 12, 244 (1971).
[5]A. van Deursen and J. Reuss, Int. J. Mass Spectrom. Ion Phys. 11, 483 (1973).
[6]A. van Deursen and J. Reuss, Int. J. Mass Spectrom. Ion Phys. (in press).

# VI EQUILIBRIUM CALCULATIONS

## VI 1 INTRODUCTION

In this chapter we present a calculation of dimer intensities obtained in supersonic expansions There are two possible limiting considerations, the dimers observed are already present in the source, in thermodynamic equilibrium, and are accelerated in the expansion Destruction during acceleration is neglected, as are processes leading to newly formed dimers On the other hand one can apply a kinetic approach, where formation and destruction processes are followed throughout the expansion The difficulty of this approach stems from the fact that the density, temperature and rate constants have to be known at all distances from the nozzle (ref 1)

We first have adopted the simple point of view and have compared the measured dimer intensities (ref 2, ch III and IV) with the equilibrium concentration in the source The comparison is performed under the assumption that the detection efficiency for dimers is twice the detection efficiency for monomers The factor two stems from the enhanced ionization efficiency for the loosely bound van der Waals complex Possible differences in detector transmission and multiplier yield are neglected The source equilibrium calculation leads to agreement with observation within a factor three for Ar, Ne, and $H_2$ For the diatomic species $N_2$ and NO the observed dependence of the dimer concentration on the stagnation pressure disagrees with the simple equilibrium theory, although the overall temperature dependence follows rather well the equilibrium predictions In the last section we discuss the experimental evidence against the simple point of view that the dimers of the onset region are formed in the source already, under equilibrium conditions Although this "source equilibrium theory" leads to semiquantitative agreement with the experimental results, the discussion indicates strongly that the observed dimers are formed downstream the nozzle We are aware that neither a source– nor a downstream equilibrium approach gives an adequate description of the properties of a molecular beam which develops from a hydrodynamical flow into a free particle stream Nevertheless, it appears that the source equilibrium gives the right dimer fraction within an order of magnitude, or even better for the noble systems The larger discrepancy found for the diatomic systems, can be explained by downstream equilibrium, i e postfabrication However, for Ne this leads to unphysically low forming temperatures of the dimer In spite of this, equilibrium theory can be used as a predictor and helps to elucidate the dimer formation process

We have not attempted to interprete our data on clusters heavier than dimers, because we know that the cluster ion signals do not correspond uniquely to neutral clusters At the same time, occurrence of larger clusters destroys the

direct correspondence of the dimer ion signal and the neutral dimer, too.

As an exception, the $He_2^+$ signal is interpreted in the onset region as originating from a neutral $He_3$ (ref. 3, ch.V). In the next section an equilibrium calculation for a He trimer is given, too.

The starting point for all calculations is (ref.4)

$$n_i/n_1^i = z_i(T) / (z_1(T))^i \qquad \text{(VI.1)}$$

Here $n_1$ ($n_2$) stands for the number density of the monomer (dimer), $z_1(T) = Z_1(T,V)/V$ ( $z_2(T) = Z_2(T,V)/V$ ) where $Z_1(T,V)$ ($Z_2(T,V)$) stands for the corresponding one particle partition function at temperature T ; V is the volume occupied by the gas. The equation is based upon ,,chemical'' equilibrium between monomers and dimers; implicitely it is assumed that the mixture of monomers and dimers can be treated as a mixture of two perfect gases. Eq. VI.1 implies that $n_2/n_1^2$ is a function of temperature only. Thus, $n_2$ is proportional to the squared source pressure $P_0^2$ in the limit of low dimer concentration. Experimentally we found this pressure dependence for $Ar_2$, $Ne_2$, and $(H_2)_2$ in the beam (ch. III,IV).

For mixed dimers one derives with $K = n_2/n_a n_b$

$$K = \left[\frac{h^2}{2\pi kT}\,\frac{(m_a+m_b)}{m_a.m_b}\right]^{3/2} \cdot \left[\sum_{v,j}(2j+1)\exp(-\varepsilon_{v,j}/kT)\right]$$

$$\left[(1/Z_{rot,a})\sum_{j_a}(2j_a+1)\exp\{-j_a.(j_a+1).B_a/kT\}\right]$$

$$\left[(1/Z_{rot,b})\sum_{j_b}(2j_b+1)\exp\{-j_b.(j_b+1).B_b/kT\}\right] \qquad \text{(IV.2)}$$

The first factor on the right hand side represents the translational part of the partition function; the second factor contains the allowed dimer vib-rot-levels $\varepsilon_{v,j}$ ; the third and fourth factor reflect the rotation of the constituent monomers. If other degrees of freedom are thermally excited, like the low lying electronic level of NO, extra factors of similar structure have to be added to the right hand side of eq. VI.2.

The summations have to be performed under the restriction

$$\varepsilon_{v,j} + j_a.(j_a+1).B_a + j_b.(j_b+1).B_b < 0 \qquad \text{(VI.3)}$$

In eq. VI.2 $m_a$ and $m_b$, stand for the mass of the constituent monomers, $B_a$ and $B_b$ for their rotational constants, with corresponding quantum numbers $j_a$ and $j_b$. It is assumed that the consituents can rotate freely (ref.5), and that their rotational states do not affect the dimer levels $\varepsilon_{v,j}$ . In the high temperature limit the rotational partition functions of both constituents $Z_{rot.a}$ and $Z_{rot.b}$ are equal to $kT/B_a$ and $kT/B_b$, respectively. Except for $H_2$, this high temperature limit is applicable to the description of our experiments for diatomic molecules. If a = b, eq. VI.2 reduces to a special case of eq. VI.1.

For the monoatomic systems the third and fourth factor are equal to unity. In that case the second factor has been evaluated semiclassically (ref. 6). One obtains for a Lennard Jones 12-6 interaction potential and for $kT>.5\varepsilon$ (ref. 7)

$$n_2 / n_1^2 = 1.78\ R_m^3\ (kT/\varepsilon)^{-1.5}\ G(Tk_0/\varepsilon) \qquad \text{(VI.4)}$$

with $G(x) = 1 + .254/x + .057/x^2 + .0107/x^3$; $\varepsilon$ and $R_m$ represent the well depth and the position of the potential minimum.

In general, eq. VI.2 must be calculated numerically, because of the coupled summations due to eq. VI.3.

## VI.2 EQUILIBRIUM THEORY FOR THE DIMER FRACTION OF INERT GAS SYSTEMS

In fig. VI.1, $\exp(\varepsilon_{0,0}/kT)$ times the internal partition function $Z_{2,int}$ is given for $Ar_2$, as a function of temperature, with $Z_{2,int} = \Sigma\exp(-\varepsilon v,j/kT)$. Because of symmetry only even values of j are taken into account in $Z_{2,int}$ (ref. 8). The steep increase at low temperatures reflects the exponential $\exp(\varepsilon_{0,0}/kT)$. At high temperatures, $Z_{2,int}$ levels off because all stable states become occupied with equal probability.

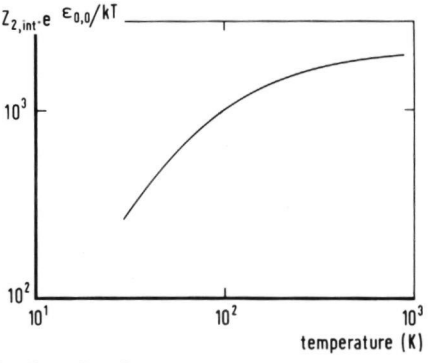


*Fig. VI.1. The internal partition function* for $Ar_2$, $Z_{2,int}$ multiplied by $\exp(\varepsilon_{0,0}/kT)$, vs. temperature.

For $Ar_2$ the energy levels $\varepsilon_{v,j}$ , are calculated using spectroscopical constants given by Docken and Schafer (ref. 9), who determined the constants for an interaction potential of $Ar_2$, obtained from differential cross section measurements by Pearson et al. (ref. 10). The level scheme is in agreement with UV absorption measurements of Tanaka and Yoshino (ref. 11), as discussed by LeRoy (ref. 12).

For $Ne_2$ similarly spectroscopical constants from Tanaka et al. (ref. 13) have been used. For $(H_2)_2$ the energy levels are calculated from a Lennard Jones 12-6 potential (ref. 14). Similarly, we could have used the high pressure infrared absorption data of Watanabe and Welsh (ref. 15), as analysed by Gordon and Cashion (ref. 16). Both level schemes yield practically indistinguishable partition functions.

The energy levels used are tabulated in appendix A1.

In all cases metastable dimers are neglected (eq. VI.3). They are assumed to dissociate before or during detection.

Mixed dimers of the Ne isotopes are observed, i.e. $^{20}Ne^{22}Ne$. From statistical symmetry arguments (ref. 8) their relative abundance compared to $^{20}Ne_2$ is expected to be twice the relative abundance of $^{22}Ne$ in $^{20}Ne$. This is confirmed by experiment.

When calculating the partition function the ortho-para species of $H_2$ have been taken into account. Above 100 K higher rotational states of $H_2$ become populated. Because the rotational energy of an excited $H_2$ molecule exceeds the binding energy of a dimer by an order of magnitude, we discard the excited molecules in eq. VI.2 according to eq. VI.3.

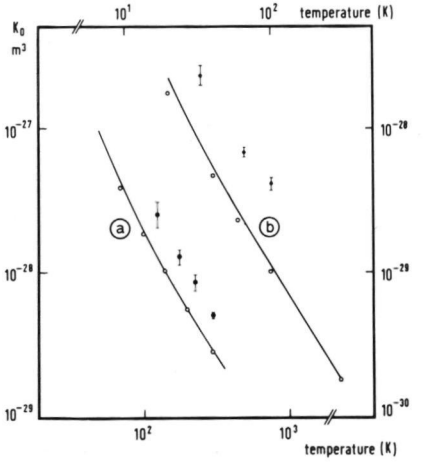


*Fig. VI.2 The equilibrium constant $K_0$ vs. temperature* for Ar (a) and Ne (b). Also shown are the values for $K_{obs}$ at different source temperatures. The open circles represent the values for $K_0$ from eq. VI.4.

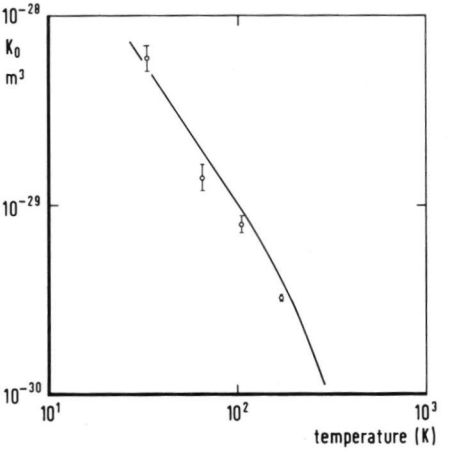


*Fig. VI.3. The equilibrium constant $K_0$ vs. temperature* for $H_2$.
At temperature between 10 K and 100 K one finds $K_0 \sim T^{-3/2}$; $K_0$ falls off more rapidly above 100 K because of excitation of higher rotational states of the monomers. A single value for $K_{obs}$ is given at each source temperature, in good agreement with $K_0$.

In fig. VI.2 we compare the calculated $K_0$ with experimental values $K_{obs}$ for Ar and Ne; $K_0 = n_2/n_1^2$ is taken at source temperature $T_0$, $K_{obs} = (I_2/I_1)/2n_1$, where $I_2/I_1$ stands for the experimental ratio of dimer and monomer intensity (see ch. III and IV); $n_1 = P_0/kT_0$ is the number density of the monomer in the source at pressure $P_0$ and temperature $T_0$; the factor 2 compensates approximately for the larger detection efficiency of the dimer with respect to that of the monomer. Besides our own calculation of $K_0$ the semiclassical results of Stogryn and Hirschfelder ( eq. VI.4) are displayed in fig. VI.2. The simple eq. VI.4, thus, yields good agreement for Ne and Ar.

We find $K_{obs} = 2\ K_0$ for Ar and $K_{obs} \simeq 3\ K_0$ for Ne.

The calculated values of $K_0$ for $H_2$ are displayed in fig. VI.3, together with our experimental values $K_{obs}$, taken from ch. IV. The experimental values are lower than the calculated ones generally, $K_{obs} \simeq 0.8\ K_0$.

Possible formation of a stable $He_2$ (ref. 17,18) has become a much discussed question recently. If there exists a bound state at all, its energy would be $\varepsilon_{0,0}/k = -0.1$ K, at maximum. In the calculation of $K_0$ this binding energy can be neglected compared to the thermal energy $kT_0$ ($T_0 = 7$K used in our experiment, ch. V). In fig. VI.4 the calculated equilibrium constant $K_0$ is displayed. The temperature dependence is purely translational, $K_0 \simeq T_0^{-1.5}$. The experimental results show no quadratic pressure dependence at all. Therefore, a range of experimental $K_{obs}$ is shown in fig. VI.4; the values even at high pressures are far too low compared to $K_0$.

In fig. VI.4 the result for a supposed $He_3$ is shown, too, $K_3 = n_3/n_1^3 \simeq T^{-3}$.

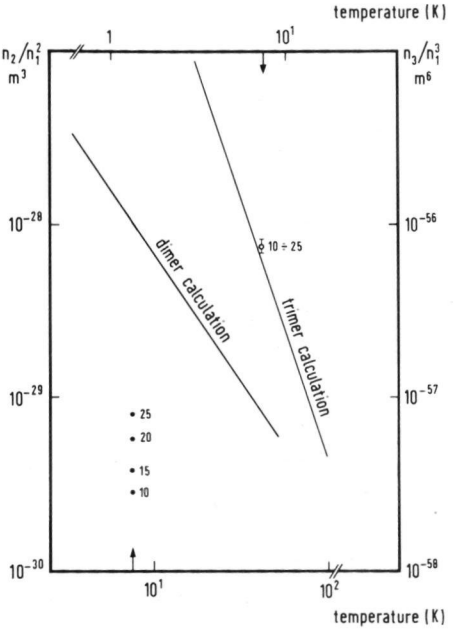


*Fig. VI.4. The equilibrium constant vs. temperature* for the smallest He cluster. The left part of the figure corresponds to the dimer calculation with $K_0 \sim T^{-3/2}$. The experimental points $K_{obs}$ are pressure dependent and far too low. The monomer density $n_1$ in the source is indicated in amagat. The right part corresponds to the trimer calculation, with $K_0 \sim T^{-3}$. The experimental $K_{3,obs}$, in fair agreement with $K_3$, assume a single value for all source pressures of interest.

Again, a single bound state with negligible binding energy is assumed, in accordance with the theoretical prediction of ref. 19. Experimentally, the $He_2^+$ signal is proportional to the third power of the source pressure, $P_0^3$. Therefore, all our $K_{3,obs}$ condense into one single point, if we take a He trimer as being responsable for the observed $He_2^+$ signal. Here, $K_{3,obs}$ is defined as $K_{3,obs} = (I_2/I_1)/3n_1^2$ with $n_1 = P_0/kT_0$. The experimental intensity ratio for $He_2^+$ and $He^+$, $I_2/I_1$, is divided by a factor 3 to compensate approximately for the larger ionization efficiency of the He trimer. The experimental $K_{3,obs}$ is in fair agreement with $K_3$.

## VI.3 EQUILIBRIUM THEORY FOR DIATOMIC SYSTEMS

For $N_2$ and NO three important features are observed, 1) the dimer intensity is more than a factor 10 lower compared to Ar, 2) the quantity $K_{obs}$ is proportional to $T_0^{-\delta}$, with $\delta > 2$, whereas $\delta \simeq 1.7$ has been found for Ar, Ne, and $H_2$, 3) $K_{obs}$ does depend on the source pressure $P_0$, whereas $K_{obs}$ is pressure independent for Ar, Ne, and $H_2$. All three properties can be explained from one single point of view, the rotational degree of freedom of the constituents of the dimer.

According to eq. VI.3 only those states are taken into account in the calculation of $K_0$ for which the sum of the rotational energies and of the end over end rotation does not exceed the binding energy for the different vibrational levels of the dimer.

The vibrational levels $\varepsilon_{v,0}$ are approximated by a J.W.K.B. – calculation for a Lennard Jones 12-6 potential with $\varepsilon$ and $R_m$ taken from ref. 20. The vibrational levels used are tabulated in appendix A 1. For all vibrational levels the rotational constant of the dimer is taken at the equilibrium distance $R_m$, i.e. $B_v = \hbar^2/m_1.R_m^2$ ($m_1$ equals the monomer mass). The monomer rotational constant is taken from ref. 21.

The influence of these two approximations is tested for Ar, where $Z_2$ from the "exact" level scheme (ref. 9) is compared to $Z_2$ for the J.W.K.B. approximated level scheme for a Lennard Jones 12-6 potential, with parameters $\varepsilon$ and $R_m$ from ref. 20. The resulting partition function $Z_2$ is 40% lower for our approximation. If $\varepsilon/k$ for the Lennard Jones potential is taken equal to 140.8 K (ref. 9) instead of $\varepsilon/k = 124$ K (ref. 20), retaining a constant value of the reduced de Broglie wavelength $\Lambda^* = h/R_m(m_1\varepsilon)^{\frac{1}{2}}$, the difference between both partition functions becomes 15%. This remaining difference is entirely due to the choise of a single value for the dimer rotational constant $B_v$, which is too large for high vibrational levels (see appendix A1).

For $N_2$ we tested the dependence of $Z_2$ on the well depth $\varepsilon$, increasing $\varepsilon/k = 91.5$ K of ref. 20 also by 13% with constant $\Lambda^*$; an increase in $Z_2$ of 50% was found at maximum. We estimate, therefore, that $K_0$, being calculated with $\varepsilon$ and

$R_m$ of ref. 20 could be 70% too small. In the following we will use this rather low value of $K_0$ only.

With the above mentioned assumptions we obtain values for $K_0$ which are two orders of magnitude lower than $n_2/n_1^2$ calculated according eq. VI.4. The resulting values are shown in fig. VI.5 for $N_2$ and NO respectively.

The tremendeous influence of the rotational degree of freedom on the equilibrium constant $K_0$ is thus put into evidence.

Also displayed are values of $K_{obs}$ for different densities $n_1 = P_0/kT_0$ ($n_1$ indicated in amagat). The discrepancy between $K_{obs}$ and $K_0$ is larger than for Ar and Ne; $K_{obs} \simeq 10K_0$.

The general temperature dependence of $K_{obs}$ is in reasonable agreement with the temperature dependence of $K_0$, for instance for $N_2$, $K_0 \simeq T^{-3.6}$, see fig. VI.5a.

The increase of $K_{obs}$ with pressure indicates that the dimers are not prefabricated in the source under equilibrium conditions, otherwise $K_{obs}$ must be pressure independent. We attribute the observed increase of $K_{obs}$ with $P_0$ to formation of dimers downstream the nozzle and to rotational cooling in the

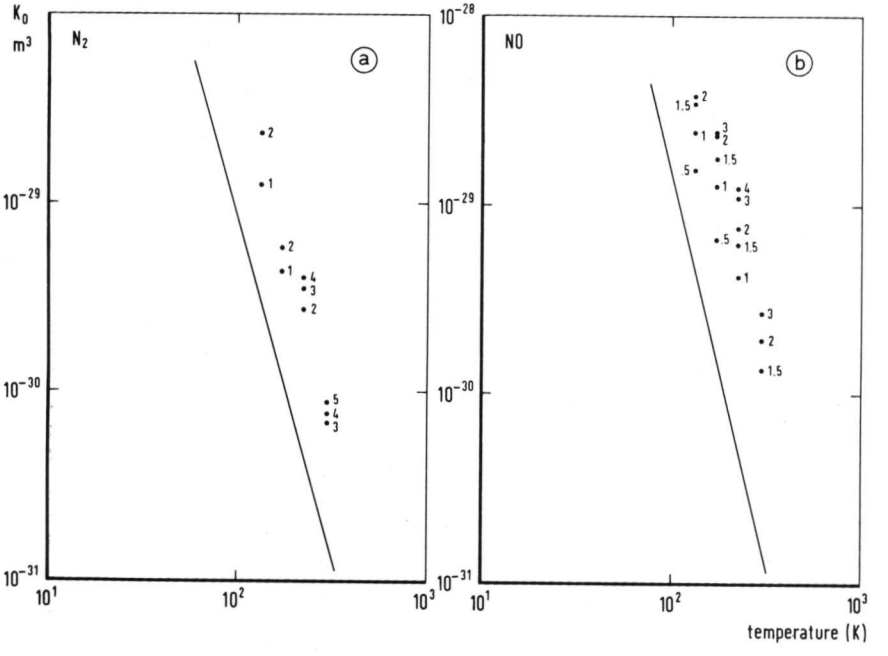


*Fig. VI.5. The equilibrium constant $K_0$ vs. temperature* for $N_2$ (a) and NO (b).
The solid lines represent the calculated $K_0$. The stronger temperature dependence here, compared to fig. VI.2, is caused by the monomer rotational degree of freedom. The values of $K_{obs}$ are given for different $n_1$, the monomer density in the source, indicated in amagat units, at four source temperatures. Because the dimer intensity is not proportional to $P_0^2$, $K_{obs}$ assumes different values at different $P_0 = n_1 kT_0$, for each $T_0$.

expanding beam. This point will be discussed in the next section. Nevertheless, the equilibrium theory is apparently capable to explain the gross features of our observations.

## VI.4. DISCUSSION

The agreement between source equilibrium calculations and the experimental values for $n_2/n_1^2$ is satisfying for Ar and Ne. The remaining discrepancy amounts to $K_{obs} = 2K_0$ for Ar, and $K_{obs} \simeq 3K_0$ for Ne. For dimers Milne and Greene (ref. 1) have introduced an extra mass separation factor (a factor 2) to deal with this discrepancy for Ar. We have investigated this mass separation on a 1:3 mixture of Ar and Ne; no enhancement of Ar was found. This does not entirely exclude mass separation for our actual 1:100 mixture of dimers and monomers, but we do not believe in the magnitude of the effect assumed in ref. 1.

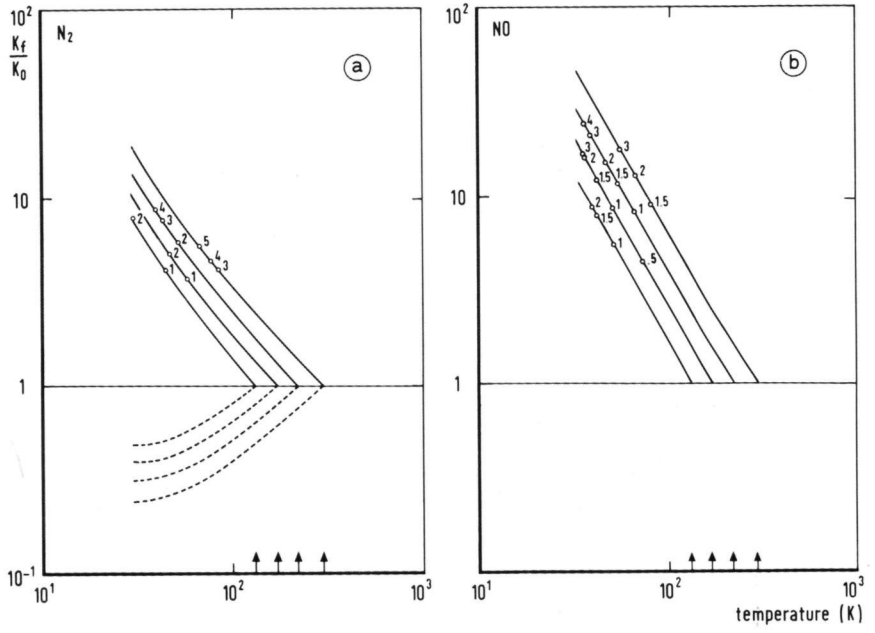


*Fig. VI.6. $K_f/K_0$ vs. temperature* for $N_2$ (a) and NO (b).
The ratio $K_f/K_0$ stands for the increase of the equilibrium dimer fraction in the isentropically expanding beam with respect to the dimer fraction in the source. The arrows on the abscissa indicate the four experimental source temperatures. As the expansion proceeds the beam temperature becomes lower and the dimer fraction increases as shown. The experimental results $K_{obs}/K_0$ are indicated by the open circles and labeled by the corresponding monomer densities in the source. From these ratios one infers formation temperatures $K_f$ which describe the observed dimer fractions, 30 K$<T_f<$100K. For $N_2$ the ratio $K_f/K_0$, calculated according to eq. VI.6 with $\varkappa = 7/5$, is indicated by the dotted line.

On the other hand, it is clear from fig. IV.1 and IV.2 that the monomer intensity departs from the extrapolated straight line $\sim P_0^1$ of the onset region, at such pressures where the dimers are observed. The origin of this deficiency may be sought in a mass separation in the expanding beam. We have corrected for this deficiency, using the extrapolated straight line values. The correction on $K_{obs}$ has negligible influence for Ar and Ne. For $N_2$ and NO it amounts to a factor 1.5 at maximum; nevertheless, it does not bring the $K_{obs}$ and $K_0$ into as close an agreement as found e.g. for Ar.

However, it is not necessary that the dimers observed are formed in the source under equilibrium conditions, only. A cooling of all degrees of freedom for monomers in a nozzle expansion has been observed many times (ref. 22). If dimers are formed downstream the nozzle and if the beam temperature has dropped before the dimer formation ends, one may expect dimer fraction quite different from the equilibrium value in the source. Hagena (ref. 7) has discussed such a "downstream equilibrium" and gives the variation of the equilibrium dimer fraction with $T_f$, the temperature downstream the nozzle which determines the finally observed dimer fraction.
The expansion from $T_0$ to $T_f$ is assumed to be isentropic. For Ar and Ne one may use eq. VI.4 to obtain

$$K_f = K_0 . (T_f/T_0)^{(5-3\varkappa)/(2\varkappa-2)} . G(kT_f/\varepsilon) / G(Tk_0/\varepsilon), \qquad \text{(VI.6)}$$

where $\varkappa$ is the specific heat ratio and $K_f = [n_2/n_1]_{T_f} . kT_0/2P_0$. In the case of noble gases $\varkappa = 5/3$ and the second factor on the right hand side is equal to unity. As G(x) is only a slowly varying function of x for $x > .5$, the dimer fraction is rather insensitive to $T_f$. To achieve agreement between $K_{obs}$ and $K_f$ we must assume a final temperature $T_f$, $T_f \simeq 60$K for Ar, for all $T_0$ between 120K and 300 K, independent of $P_0$. For Ne the downstream equilibrium would lead to $T_f < 20$ K; for this low $T_f$ our basic assumptions are not longer valid.

For Ar, Ne and $H_2$ the close agreement between $K_{obs}$ and $K_f$ is caused by the rather weak dependence of the dimer fraction on $T_f$; it does not prove that the observed dimers are already formed in the source.

For $H_2$ good agreement is found between $K_0$ and $K_{obs}$. This stems from the near independency of $K_f$ on $T_f$ for $T_f > 10$K, due to the small binding energy of the $H_2$ dimer levels. Thus, any $T_f$ with $10\ K < T_f < T_0$ would fit to our measurements.

For the diatomic systems $N_2$ and NO the discussion of the experimental results in the light of a source equilibrium theory is problematic, because the dimer intensity is not found to be proportional to $P_0^2$. The value of $K_{obs}$ changes about a factor 2 for $N_2$ (a factor 5 for NO) at fixed $T_0$, if the pressure $P_0$ is varied from the detection limit up to $P_1$ (see ch. III and IV). A large spread of experimental points is caused by the pressure dependence, $K_{obs} \sim P_0^{.5}$ for $N_2$ and $K_{obs} \sim P_0^{.8}$ for NO.

As in the case of Ar and Ne, we have investigated the consequences of dimer formation downstream the nozzle. The new element for the diatomic molecules is the strong influence of the rotational cooling on $Z_2$ in eq. VI.2. Using eq. VI.2 one can derive a relation for $K_f$ for diatomic systems analogously to eq. VI.6. In fig. VI.6 calculated values for $K_f/K_0$ are given for different source temperatures. Hagena, who has not expicitely taken into account the rotational cooling, finds a behaviour completely different from our calculations for $N_2$ (see fig. VI.6). For NO, the cooling of the electronic degree of freedom must also be taken into account. The slightly larger temperature and pressure dependence of $K_{obs}$, as displayed in fig. VI.6 is attributed to the electronic cooling.

In contrast to the noble systems the influence of $T_f$ on the dimer fraction is very pronounced in the case of $N_2$ and NO due to the presence of internal degrees of freedom. The observed pressure dependence of $K_{obs}$ therefore indicates strongly that the dimers are formed downstream the nozzle, at temperatures $T_f$ between 30 K and 100 K (see fig. VI.6).

REFERENCES CHAPTER VI


1 T. A. Milne and F. T. Greene, J. Chem. Phys., *47* (1967) 4095
T. A Milne, A. E. Vandegrift and F. T. Greene, J. Chem. Phys., *52* (1970) 1552
2. A. v. Deursen, A. v. Lumig and J. Reuss, Int. J. Mass Spectrom. Ion Phys , *18* (1975) 129, chapter III of this thesis.
3 A P. J. v. Deursen and J. Reuss, J. Chem. Phys., *63* (1975) 4559, chapter V of this thesis.
4 see e g. F Mandl, "Statistical Physics", Wiley, New York (1971)
5. Ch. A. Long, G. Henderson and G. E. Ewing, Chem. Phys., *2* (1973) 485
6. D. E Stogryn and J. O. Hirschfelder, J. Chem Phys., *31* (1959) 1531 and J. Chem. Phys., *33* (1960) 942
7 O. F. Hagena, Entropie, *42* (1971) 42
8. see e.g. N. Davidson, "Statistical Mechanics", McGraw-Hill, New York (1962)
9. K. K. Docken and T. P. Schafer, J. Mol. Spectrosc., *46* (1973) 454
10. J. M. Pearson, P E. Siska and Y. T. Lee, J. Chem. Phys., *56* (1971) 5762
11 Y. Tanaka and K. Yoshino, J. Chem. Phys., *53* (1970) 2012
12. R. J LeRoy, J. Chem. Phys., *57* (1972) 573
13. Y. Tanaka and K Yoshino, J. Chem. Phys., *57* (1972) 2964
Y. Tanaka, K. Yoshino and D. E Freeman, J. Chem. Phys., *59* (1973) 564
14. J. D. Poll, private communication
15. A. Watanabe and H. L. Welsh, Phys. Rev. Lett., *13* (1964) 810
16 R. G. Gordon and J. K. Cashion, J. Chem. Phys., *44* (1966) 1190
17. H. G. Bennewitz, H. Buse, H D. Dohman, D. E. Oates and W. Schrader, Z. Physik, *253* (1972) 435
18. J H. Farrar and Y. T. Lee, J. Chem. Phys., *56* (1972) 5801
19. L. W. Bruch and I. J. McGee, J. Chem. Phys., *59* (1973) 409
T. K. Lim and M. A. Zuniga, J. Chem. Phys., *63* (1975) 2245
20. J. O Hirschfelder, C. F. Curtiss and R. B. Bird, "Molecular Theory of Gases and Liquids", Wiley, New York (1965)
21. G. Herzberg, "Molecular Spectra and Molecular Structure", D. v. Nostrand, New York (1954)
22. see e.g. J. B. Anderson in "Molecular Beams and Low Density Gasdynamics", ed. P. Wegener, M. Dekker, New York (1974)

# VII MIXED DIMERS

## VII 1 INTRODUCTION

Continuing our investigation of dimer production (ref 1) we have tried to detect mixed dimers in nozzle beams of mixtures, NeAr and HeNe dimers were observed with sufficient intensity to determine the total collision cross section A similar attempt for $H_2Ar$ was partially hampered by the circumstance that the corresponding $HAr^+$ ion must be detected on the wing of the thousand times larger $Ar^+$ peak Our search for $H_2He$, $H_2Ne$ and HeAr dimers was not successful, due to masking ion peaks, $H_3^+$ for $HHe^+$, $^{21}Ne^+$ for $H^{20}Ne^+$, and $CO_2^+$ for $HeAr^+$

For the Ne-Ar mixture (3 Ne 1 Ar in the source) we observe an optimum $NeAr^+$ signal of about 0 1% of the $Ar^+$signal with a signal to noise ratio S/N = 30, at a time constant $\tau$ = 1 sec A similar result is obtained for the He-Ne mixture At the moment these optimum signals seem too small for electric beam resonance measurements, which appear interesting in view of recent discussions of the electric dipole moment of these mixed inert gas dimers (ref 2)

The existence of an $H_2He$ dimer is questionable (ref 3), The situation can be compared to that of the He dimer Our results do not throw new light on this problem

A positive aspect of the mixed clusters and their mass spectrometric detection is the low probability for fragmentation of larger clusters to the mixed dimer ion For instance, using the Ne-Ar mixture, signals of $Ar_3^+$– and $Ar_4^+$–ions are found, but no signals of $NeAr_2^+$-ions Even conceding that neutral $NeAr_2$ is present in the beam, $NeAr^+$ will be formed as fragment ion with smaller probability than $Ar_2^+$ In complete agreement herewith we observe a constant collision cross section for the $NeAr^+$ parent up to pressures substantially higher than those at which the $Ar_2$– $Ar_2^+$ correspondence breaks down, i e $P_I$ (sect VII 3), at these high pressures the $NeAr^+$ signal goes through a maximum For $HeNe^+$ a constant collision cross section is observed up to pressures where the $HeNe^+$ signal has dropped already to 3 of its maximum value

As will be shown in sect VII 4 the observed mixed dimer intensities can be fairly well predicted from a source equilibrium calculation

Concerning the production of pure dimers from gas mixtures, e g $Ar_2$ from the Ne-Ar mixture, we observe a significant increase through the presence of the lighter gas compared to the dimer intensity from pure gases, at the same partial pressure and temperature in the source This increase points definitively in the direction of dimer formation downstream the nozzle, where, due to the extra acceleration of the beam molecules by the light carrier gas, the formation temperature $T_f$ is lower than for pure gas jets, see sect VII 4 Similar observations have been reported in ref 4

In fig. VII.1,2a and 2b the intensities are displayed for the mixed gases as a function of the source pressure $P_0$. The mixtures have been prepared by us from commercial pure gases; we have used 1:3 mixtures of Ar in Ne, Ne in He and Ar in $H_2$.

The monomer signals nearly coincide for Ne-Ar and He-Ne mixtures.

When the difference in detection efficiency is taken into account (see appendix A 2) we find no enhancement of the heavier monomer in the beam. On the other hand, for the $H_2$-Ar mixture with its large mass difference between the components, an order of magnitude less $H_2$ is measured with respect to Ar. This cannot be explained by a difference in detection efficiency. The light carrier gas is lost from the central beam by collisions with the heavier component (ref. 4). As soon as the $Ar_2$ signal appears, the $H_2$ monomer signal becomes practically independent of $P_0$, presumably due to increasing losses caused by the Ar dimer formation process. Energy is liberated in the dimer formation process; corresponding linear momentum is mainly imparted to the lighter component of the mixture.

For a pure Ar monomer beam a signal from $Ar^{++}$ ions is observed, of about 10% of the $Ar^+$ signal, at an electron bombardment energy of 130 eV. In fig. VII. 1 the intensity of $Ne^+$ is corrected for this $Ar^{++}$ signal (about 10% decrease).

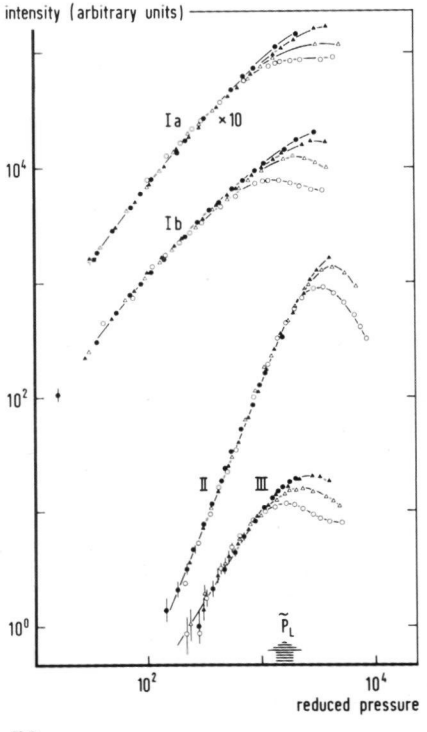


*Fig. VII.1. Intensity vs. reduced pressure* for Ne-Ar.
The $Ne^+$ intensity (Ia,displayed multiplied by a factor 10) nearly coincides with the $Ar^+$ intensity (Ib). Both monomer intensities are proportional to $P_0^{\alpha_1}$ at low pressures, with $\alpha_1 = 1.0 \pm .1$. For the $Ar_2^+$ (II) and $NeAr^+$ (III) intensity similar proportionalities hold with exponents $\alpha_2 = 2.5 \pm .2$ and $\alpha_3 = 1.6 \pm .2$, respectively. The intensities are measured at different source temperatures, $T_0 = 296$ K (●), $T_0 = 190$ K (▲), $T_0 = 148$ K (△), and $T_0 = 108$ K (O). The abscissa gives the true pressure in torr for $T_0 = 190$ K. At other temperatures reduction factors $P_0/P_{red}$ are applied for each ion mass (table VII.1.) The shaded area indicates the reduced pressure $\tilde{P}_L$ at which the $Ar_2$ signal becomes contaminated by fragments of larger clusters.

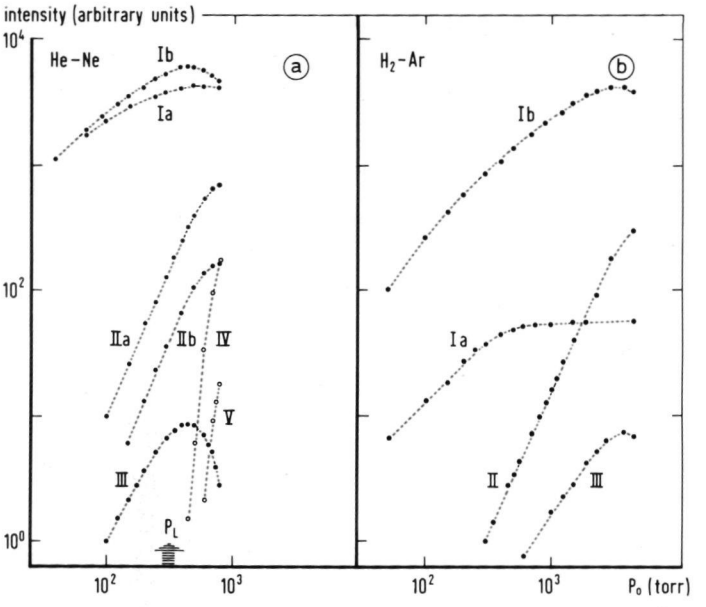


*Fig.VII.2. Intensity vs. source pressure* for He-Ne (a) and $H_2$-Ar (b).
For He-Ne (at source temperature $T_0 = 31$ K) the intensities are shown of the ions $He^+$ (Ia), $^{20}Ne^+$ (Ib), $^{20}Ne_2^+$ (IIa), $^{20}Ne^{22}Ne^+$ (IIb); at low pressures the ion signals are proportional to $P_0{}^{\alpha_m}$, with $\alpha_m \approx 1$ (I), $\alpha_2 = 2.3 \pm .2$ and $\alpha_3 = 1.5 \pm .2$ (III). Also shown are the intensities for $Ne_3^+$ (IV) and $Ne_4^+$ (V). At the pressure $\tilde{P}_L$ fragment ions of larger clusters start to contribute to the $Ne_2^+$ signal. For $H_2$-Ar at source temperature $T_0 = 173$ K, the intensities are shown of $H_2^+$ (Ia), $Ar^+$ (Ib), $Ar_2^+$ (II), and $HAr^+$ (III). At low pressures the ion signals rise proportionally to $P_0{}^{\alpha m}$, with $\alpha_{1a} = 1. \pm .2$, $\alpha_{1b} = 1. \pm .1$, $\alpha_2 = 2.3 \pm .1$, and $\alpha_3 = 1.5 \pm .2$, respectively.

In fig. VII.1 the pressure scale is the true one for $T_0 = 190$ K; for other temperatures the pressure scale is reduced for each ion signal by the factors $P_0/P_{red}$, given in table VII.1.

The $^{20}Ne\ ^{40}Ar^+$ ion signal could be contaminated by $Ar_3^{++}$ ions, possessing the same e/m ratio. However, for a pure Ar beam no $Ar_3^{++}$ has been found; therefore we exclude this possibility.

We have not found signals of $^{22}Ne^{40}Ar^+$ or $^4He^{22}Ne^+$ ions; their intensity can be estimated to be an order of magnitude lower than that observed for $^{20}Ne^{40}Ar^+$ and $^4He^{20}Ne^+$ ions; this is beneath our detection limit.

Our mass spectrometer has a limited suppression of neighbouring mass peaks; for a pure Ar beam about .03% of the $Ar^+$ signal is measured at the mass-setting for $HAr^+$. The mixed dimer signal in the case of $H_2$-Ar, $HAr^+$, must be detected on the wing of a thousand times larger $^{40}Ar^+$ monomer peak. Therefore, the intensities of fig.VII.2b should be taken with some reserve. However, the scattering results of the next section prove that a mixed dimer signal is present. No attempt with a $D_2$-Ar mixture has been made yet.

Dimers of the heavier component in the mixture are detected. In contrast to the case of pure gases, their intensity is proportional to $P_0^{\alpha}$ , with $\alpha_2$ larger than 2 (see caption of fig. VII. 1 and 2); for pure gases $\alpha_2 = 2$ has been found (ref. 1, ch. III and IV). At the same source temperature and partial source pressure the dimer intensity from the mixture has increased with respect to that of the pure gas. For a discussion see sect. VII.4.

The monomer intensities are about proportional to $P_0$ at low pressures; the mixed dimer signals have pressure exponents $\alpha_1$ smaller than 2. The exact values are given in the captions.

TABLE VII.I

| | | $T_0$ (K) | | | | | | $\beta_1$ |
|---|---|---|---|---|---|---|---|---|
| | | 108 | 148 | 190 | 296 | 120 | 210 | |
| $Ne^+$, $Ar^+$ | (I) | .65 ± .1 | .8 ± .1 | 1 | 1.5±.1 | .7 | 1.1 | .85 ± .1 |
| $Ar_2^+$ | (II) | .35 ± .02 | .55 ± .03 | 1 | 2.1±.1 | .4 | 1.4 | 2 1 ± .1 |
| $NeAr^+$ | (III) | .47 ± .05 | .65 ± .07 | 1 | 1.6±.1 | .5 | 1.2 | 1.6 ± .1 |

**Table VII. 1 Reduction factors $f=P_0/P_{red}$ for Ne-Ar**
**The values for f at $T_0$= 120 K and $T_0$= 210 K have been interpolated, using the approximation $f \propto T_0^{\beta_1}$. The values for $\beta_1$ are given in the last column.**

VII 3 SCATTERING

In fig. VII.3 the total collision cross sections vs. reduced source pressure are displayed relative to the Ar monomer cross section, for the different ion signals of the Ne-Ar mixture; He was used as scattering partner. The cross sections at three different source temperatures $T_0$ = 120, 210 and 296 K are collected in one figure by a similar reduction of the pressure scale as for the intensities; for $T_0$ = 120 and 210 K interpolated reduction factors are used, see table VII.1. The experimental cross sections are corrected for the finite angular resolution following ref. 5.

At low pressures all cross sections are independent of $P_0$, indicating a direct correspondence between ions and neutrals.

The ratio of the cross section $\sigma_{Ar}/\sigma_{Ar}$ is found to be 1.52± .02, with He as target molecule. The cross section of the mixed dimer $\sigma_{NeAr}$ , is seen to be (1.61 ± .02) times $\frac{1}{2}(\sigma_{Ar} + \sigma_{Ne})$.

With Ar as scattering partner we find for $\sigma_{Ar}/\sigma_{Ar} = 1.36 \pm .02$ and $\sigma_{NeAr} = (1.45 \pm .02).\ \frac{1}{2}(\sigma_{Ar} + \sigma_{Ne})$ at a source temperature $T_0$ = 210 K.

For the $Ar_2^+$ signal a source pressure $\tilde{P}_L$ can be defined in fig. VII.3; at $\tilde{P}_L$ the cross section starts to rise above its constant low pressure value. The pressure $P_L$ is 500 torr for $T_0$ = 120 K, 1800 torr for $T_0$ = 210 K; for $T_0$ = 294 K no rise of the $Ar_2^+$ cross section is yet observed, i.e. $P_L > 4000$ torr. Indicated in fig. VII.1 and 3 is $\tilde{P}_1$ , obtained from the aforementioned $P_L$ values and the reduction factors of table VII.1 for the $Ar_2^+$ signal.

The partial pressure for Ar at $P_l$ is roughly equal to $\frac{1}{2}P_l$ found for pure Ar (cf. ch. III), in accordance with ref.4.

In fig. VII.4a and 4b the cross section for the He-Ne and the $H_2$-Ar mixture are given each for one source temperature ($T_0$ = 31 K and $T_0$ = 90 K, respectively), and one scattering partner (He and Kr, respectively). Here too, the cross sections displayed are corrected for the finite angular resolution. For the $He^+$, $Ne^+$, and $HeNe^+$ signal the cross sections are again independent of $P_0$. From the constant behaviour of $\sigma_{HeNe}$ we infer that no larger mixed clusters, if present at all, contribute to the $HeNe^+$ signal. One obtaines $\sigma_{HeNe} = (1.83 \pm .06).\frac{1}{2}(\sigma_{Ne} + \sigma_{He})$ with He as scattering partner.

At $P_0 < 300$ torr the $Ne_2$ cross section is measured, yielding $\sigma_{Ne_2} / \sigma_{Ne} = 1.75 \pm .06$. Here, the partial Ne pressure at $P_l$ = 300 torr is about equal to $P_l$ in the pure Ne case of ch. IV. For $P_0 > P_L$ the dimer ion cross section rises to values near to those of the cross section for the larger cluster ions, $Ne_3^+$ and $Ne_4^+$.

In order to obtain larger mixed dimer signals and to reduce the influence of the limited mass separation (see sect. VII.2) we have used a different source temperature and gas mixture in the measurement of the cross sections of $H_2$-Ar ($T_0$ = 90 K vs. $T_0$ = 173 K used for the intensities in fig. VII.2b, and a 8:1 mixture vs. 3:1). As in fig. VII.2b the $H_2^+$ ion signal assumes a nearly constant value over the pressure range where dimer signals are present; this constant signal is about 10% of the $Ar^+$ signal (vs. 1.5-3% in fig. VII.2b). At a source

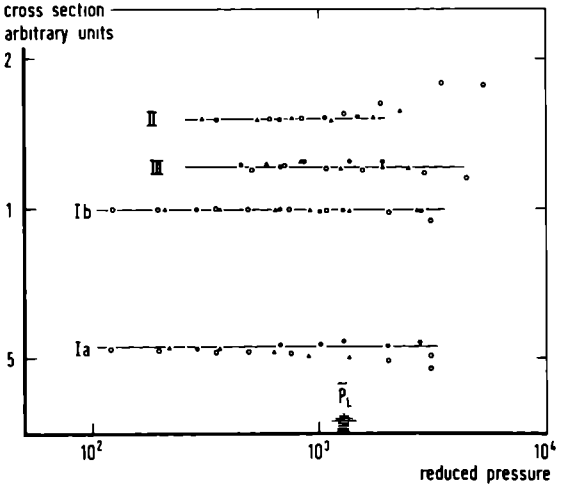


caption to fig VII.3

*Fig. VII.3. Apparent cross section vs. reduced pressure* for the Ne-Ar mixture with He as scattergas. The cross sections are diplayed relative to the Ar monomer cross section; they are measured at source temperatures $T_0$ = 296 K (▲), $T_0$ = 210 K (•), and $T_0$ = 120 K (O); for the reduction of the pressure scale interpolated $P_0/P_{red}$ values are used, see table VII.1. From $P_{red} < \bar{P}_l$ the $Ar_2$ cross section is obtained. For NeAr the results are independent of pressure over the whole pressure range.

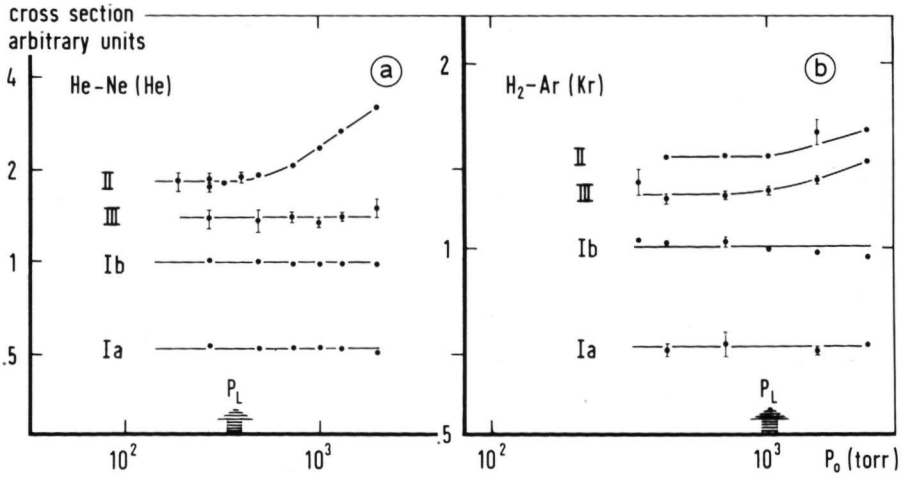


*Fig. VII.4 Apparent cross section vs. source pressure* $P_0$, (a) for a 3:1 He-Ne and (b) for a 8:1 $H_2$-Ar mixture with He and Kr as target gas, at temperatures $T_0$ = 31 K and 90 K, respectively. In the left part the $He^+$ (Ia), $Ne^+$ (Ib), and $HeNe^+$ (III) attenuations correspond for all pressures, those for $Ne_2^+$ (II) only for $P_0 < P_L$, to cross sections of well defined neutral particles.
In the right part the attenuations of $H_2^+$ (Ia), $Ar^+$ (Ib), $Ar_2^+$ (II) and $HAr^+$ (III) correspond each to a unique neutral parent for $P_0 < P_L = 10^3$ torr. At pressure $P_0 > P_L$ larger clusters contribute to both dimer signals.

pressure $P_0$ = 1000 torr both the $Ar^+$ and the $HAr^+$ ion signal go through a maximum; the maximum $Ar_2$ and HAr signal are 10% and 2% of the $Ar^+$ signal, respectively. The signal to noise ratio of the $HAr^+$ ion signal here, is 50, at a time constant of 1 sec.

From fig. VII.4b one infers a constant cross section for all ion signals at source pressures $P_0 < 1000$ torr. One obtaines $\sigma_{Ar_2}/\sigma_{Ar} = 1.35 \pm .02$ and $\sigma_{H_2Ar} = (1.45 \pm .02).\frac{1}{2}(\sigma_{H_2} + \sigma_{Ar})$. Due to the contribution of the $Ar^+$ signal to the $HAr^+$ signal as explained in the introduction, we present the cross section of the $H_2Ar$ dimer as a lower limit; the value is estimated to be too low by 2% at maximum.
At $P_0 > 1000$ torr the cross section for the $Ar_2^+$ and the $HAr^+$ signal starts to rise, due to the admixture of larger clusters. For $Ar_2^+$ this rise has been observed earlier (ref.1a); for $HAr^+$ this rise is the only indication in our investigation to the existence of larger mixed clusters. At the same pressures, signals of $H_3^+$ ions are detected too.
The decrease of the monomer cross section for Ar has been dealt with in an earlier paper (ref.1a).

For a comparison of the observed mixed dimer concentration of NeAr and the equilibrium concentration in the source we calculated the partition function $Z_{mix}$ ; the vibrational energy have been calculated by us in the J.W.K.B. approximation, using $\varepsilon$ and $R_m$ values for the Lennard-Jones 12-6 potential from ref. 6, see appendix A1. The rotational constant B has been taken at the equilibrium position of the two atoms, for all 5 vibrational levels. The resulting partition function is estimated to give values 40% too small. The estimate is based on similar $Ar_2$ results (sect. VI.2). From the partition functions the equilibrium constant $K_0 = n_{NeAr} / n_{Ne} \cdot n_{Ar}$ is calculated as a function of the source temperature $T_0$.

The experimental intensity ratio $I_{NeAr} / I_{Ar}$ is divided by 1.25 to compensate for the increased detection efficiency, and by the calculated neon density in the source, to obtain values for $K_{obs}$ . For a fixed source temperature $T_0$ the intensity ratios are used only for pressures lower than $P_0$, where the intensities reach their maxima (onset region). The resulting $K_{obs}$ values are independent of the source pressure $P_0$ to within 10%. Therefore in fig. VII.7 only one point is given for each $T_0$. We find $K_{obs} \simeq K_0$.

Similarly, we compared the $Ar_2$ concentration with the data for pure Ar

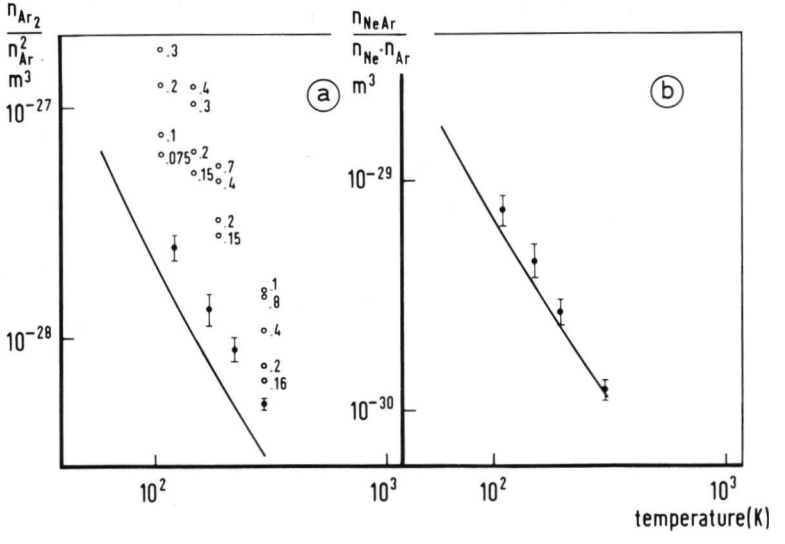


caption to fig. VII.5

*Fig. VII.5 Equilibrium constant vs. temperature.*

In the left part (a) the calculated curve $K_0$ is taken from sect. VI.2; the dots indicate the values for $K_{obs}$ for $Ar_2$ from pure Ar (see fig. VI.2). The open circles indicate the values for $K_{obs}$ for $Ar_2$ from the Ne-Ar mixture; $n_1$ stands for the partial Ar density in the source (in amagat). In the right part the dots correspond to the values of $K_{obs}$ for NeAr, which are in good agreement with $K_0$ (solid line).

from sect. VI.2, for pressures lower than $P_I$ (see sect. VII.3). In the onset region the $Ar_2^+$ intensity is proportional to $P_0^{2.5}$; consequently, the values for $K_{obs}$ are pressure dependent. In fig. VII.7 we give the values at different pressures, as indicated in the caption.

With respect to sect. VI.2 an increase of the experimental dimer concentration is found, which amounts to a factor 4, at maximum. Thus, $K_{obs}$ is pressure dependent and 4 to 8 times larger than $K_0 = n_{Ar}/n_{Ar}^2$. Both effects are attributed to an extra cooling during expansion due to the presence of the lighter Ne. They indicate strongly that the dimers observed are produced during the expansion.

The fact that $K_{obs} \simeq K_0$ for NeAr, while large discrepancies occur for $Ar_2$ from the Ne-Ar gas mixture, can be explained as follows; the NeAr dimer fraction is rather independent of the temperature $T_f$, whereas for $Ar_2$, with its two times larger potential minimum $\varepsilon$, this temperature $T_f$ forms a very critical parameter. As discussed in sect. VI.4, the dimers are assumed to be formed downstream the nozzle at an effective equilibrium temperature $T_f < T_0$. Then $K_{obs} = K_f$, with

$$K_f = K_0 \; G(kT_f/\varepsilon)/G(kT_0/\varepsilon)$$

(sect. VI.4), where

$$G(x) = 1 + .254/x + .057/x^2 + .0107/x^3$$

is a function weakly dependent on x for $x \geq .5$.

For $Ar_2$ with it large $\varepsilon$-value the condition $x \geq .5$ is not fulfilled.

For the other mixed dimer $H_2Ar$ and HeNe the results in general are similar and give no new insights; they do not yet justify an extensive calculation.

REFERENCES CHAPTER VII


1 a/A v Deursen, A v Lumig and J Reuss, Int J Mass Spectrom Ion Phys , *18* (1975) 129, chapter III of this thesis
b/ to be published, chapter IV of this thesis
2 R L Matcha and R K Nesbet, Phys Rev , *160* (1967) 72
H B Levine, Phys Rev , *160* (1967) 159
3 R Gengenbach and Ch Hahn, Chem Phys , L *15* (1972) 604
4 E W Becker, R Klingelhofer, and P Lohse, Z Naturforsch , A *17* (1962) 432
5 F v Busch, Z Physik, *193* (1966) 412
6 B N Srivastava and K P Srivastava, J Chem Phys , *30* (1969) 984

# VIII MEASUREMENTS OF TOTAL COLLISION CROSS SECTION FOR DIMERS OF SIMPLE ATOMS AND MOLECULES IN THE GLORY- AND TRANSITION REGION.

## VIII.1. INTRODUCTION.

In this communication we present a survey of total collision cross sections for van der Waals dimers of the inert gases Ar and Ne, the molecules $H_2$, $N_2$, NO, $O_2$, $CO_2$, and $C_2H_4$, and for mixed dimers NeAr, HeNe and $H_2Ar$. Most of the measurements of the dimer cross sections, $\sigma_2$, relative to the corresponding monomer cross section, $\sigma_1$, have been described before (ref.1, 2, 3, ch. III, IV and VII). For a complete review, we have added the results for the He trimer (ref. 4, ch.V) and our unpublished results for the $CO_2$ and $C_2H_4$ dimers.

The dimers are produced in a nozzle beam and are detected by a mass spectrometer. The total collision cross section is determined from the attenuation of the beam by a target gas (Ar, Kr or He) in a scattering chamber (at 80K for Ar and He, 200K for Kr).

In fig. VIII.1 all ratios $\sigma_2/\sigma_1$ are collected and plotted vs. the reduced velocity $v_{red} = \hbar v/\varepsilon R_m$. For mixed dimers the average value of both monomer cross sections is taken instead of $\sigma_1$. The systems investigated are summarized in table VIII.1. The relative scattering velocity v is calculated by $v = (v_1^2 + \alpha_s^2)^{1/2}$ (cf. ref. 5); for the beam velocity $v_1$ full isentropic expansion is assumed (ref. 6); the velocity $\alpha_s$ is the thermal velocity of the target molecules in the scattering chamber. The f.w.h.m. spread in relative velocity is about equal to $\alpha s$.

The values for $\varepsilon$ and $R_m$ are taken from a Lennard Jones interaction potential of monomer (the heavier monomer for mixed dimers) and target molecules (ref. 7, see table VIII.1).

A correction to $\sigma_2/\sigma_1$ for the finite angular resolution is applied following ref. 8. The absolute value of the total cross section, required for the calculation of the correction, is determined from Swedenburg et al. (ref. 9) and Gengenbach et al. (ref. 10), and our relative measurements.

The correction formula of ref.8 has been derived under the assumptions $v_1/\alpha_s \geq 2$ and $\sigma_1 \propto v^{-2/5}$. Consequently, this correction is uncertain for He as target molecule. Due to lack of a better procedure, it is applied, nevertheless. The fact that the experimental results taken with He in the scatterbox do not show any striking deviation in fig. VIII.1 has helped us to subdue our scruples. In table VIII.1 both measured and corrected values of $\sigma_2/\sigma_1$ are given.

Because of the large spread in relative velocity we do not observe a glory type velocity dependence of $\sigma_2/\sigma_1$. The monomers and dimers in the beam have essentially the same velocity. The spread in relative velocity is pratically entirely due to the thermal velocity of the target gas $\alpha_s$; the correction factor for the total collision cross section to deal with this spread is equal for both monomers and dimers, leaving the ratio $\sigma_2/\sigma_1$ unchanged.

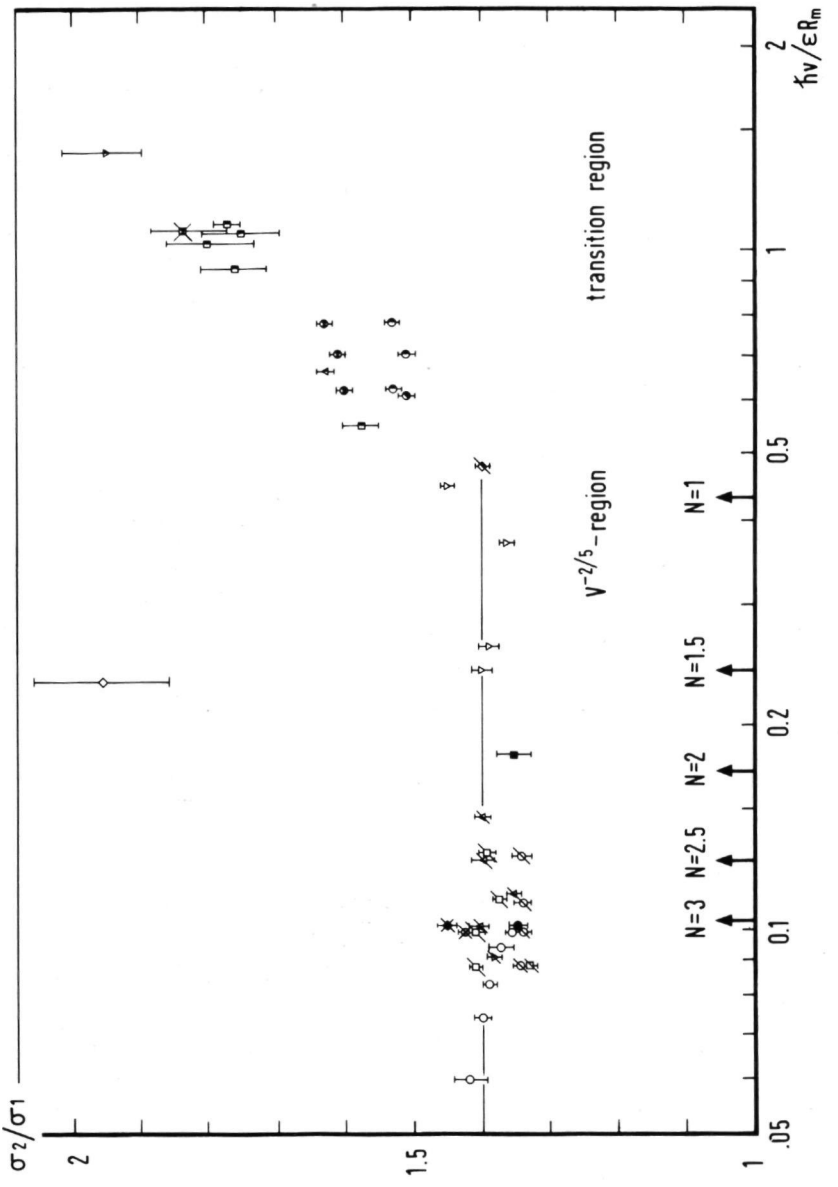


*Fig. VIII.1. Cross section ratio $\sigma_2/\sigma_1$ vs. reduced velocity.*
The explanation for the symbols corresponding to the different systems is given in table VIII.1.

TABLE VIII 1

| Beam | symbol | $T_0$ (K) | $v_i$ (m/sec) | scatter gas | $\alpha_s$ (m/sec) | v (m/sec) | $\sigma_2/\sigma_1$ eff | $\Delta C_\gamma$ | $\sigma_\infty/\sigma_1$ corr | $\hbar v/\varepsilon R_m$ | ref |
|---|---|---|---|---|---|---|---|---|---|---|---|
| Argon | ○ | 294 | 553 | Ar | 182 | 582 | 1 34 ± 03 | 1 024 | 1 37 ± 03 | 093 | a |
| | | 223 | 481 | Ar | 182 | 515 | 1 36 ± 02 | 1 022 | 1 39 ± 02 | 083 | a |
| | | 173 | 424 | Ar | 182 | 462 | 1 37 ± 02 | 1 019 | 1 40 ± 02 | 074 | a |
| | | 123 | 358 | Ar | 182 | 401 | 1 40 ± 04 | 1 016 | 1 42 ± 04 | 057 | a |
| Argon | ◑ | 294 | 699 | He | 577 | 907 | 1 45 ± 02 | < 1 052 > | < 1 53 ± 02 > | 78 | b |
| in Ne Ar (3 1) | | 210 | 591 | He | 577 | 826 | 1 44 ± 02 | < 1 050 > | < 1 51 ± 02 > | 70 | b |
| | | 120 | 447 | He | 577 | 730 | 1 45 ± 02 | < 1 052 > | < 1 53 ± 02 > | 62 | b |
| | ○ | 210 | 591 | Ar | 182 | 618 | 1 28 ± 02 | 1 063 | 1 36 ± 02 | 099 | a |
| Argon in $H_8$ Ar (8 1) | ● | 90 | 776 | Kr | 204 | 802 | 1 27 ± 02 | 1 059 | 1 35 ± 02 | 10 | f |
| Neon | ◨ | 100 | 456 | He | 577 | 735 | 1 72 ± 02 | < 1 026 > | < 1 77 ± 02 > | 1 09 | b |
| | | 65 | 368 | He | 577 | 684 | 1 75 ± 06 | < 1 028 > | < 1 80 ± 06 > | 1 02 | b |
| | | 33 | 264 | He | 577 | 634 | 1 71 ± 04 | < 1 036 > | < 1 77 ± 04 > | 94 | b |
| | ■ | 100 | 456 | Kr | 204 | 500 | 1 30 ± 05 | 1 036 | 1 35 ± 05 | 18 | c |
| Neon in He Ne (3 1) | ◨ | 31 | 402 | He | 577 | 703 | 1 71 ± 06 | < 1 026 > | < 1 75 ± 06 > | 1 05 | b |
| He | ◇ | 7 | 270 | Ar | 182 | 326 | 1 95 ± 10 | 1 008 | 1 97 ± 10 | 24 | b |
| $H_2$ | ▽ | 166 | 1858 | Ar | 182 | 1867 | 1 54 ± 04 | 1 007 | 1 55 ± 04 | 58 | b |
| | | 100 | 1442 | Ar | 182 | 1453 | 1 44 ± 04 | 1 006 | 1 45 ± 04 | 44 | b |
| | | 65 | 1163 | Ar | 182 | 1177 | 1 35 ± 02 | 1 005 | 1 36 ± 02 | 37 | b |
| | | 30 | 790 | Ar | 182 | 810 | 1 38 ± 03 | 1 004 | 1 39 ± 03 | 26 | b |
| | | 26 | 736 | Ar | 182 | 758 | 1 40 ± 03 | 1 002 | 1 40 ± 03 | 24 | b |
| | ▼ | 26 | 736 | He | 577 | 929 | 1 91 ± 06 | < 1 025 > | < 1 96 ± 06 > | 1 38 | e |
| $N_2$ | ⊿ | 294 | 782 | Ar | 182 | 803 | 1 33 ± 02 | 1 053 | 1 40 ± 02 | 146 | f |
| | | 220 | 676 | Ar | 182 | 700 | 1 34 ± 03 | 1 046 | 1 40 ± 03 | 127 | f |
| | | 173 | 600 | Ar | 182 | 626 | 1 30 ± 02 | 1 041 | 1 35 ± 02 | 113 | f |
| | | 133 | 526 | Ar | 182 | 557 | 1 35 ± 03 | 1 042 | 1 41 ± 03 | 101 | f |
| | ▲ | 173 | 600 | He | 577 | 832 | 1 57 ± 02 | < 1 045 > | < 1 64 ± 02 > | 66 | d |
| NO | ⊘ | 294 | 756 | Ar | 182 | 777 | 1 27 ± 03 | 1 055 | 1 34 ± 03 | 127 | f |
| | | 220 | 654 | Ar | 182 | 678 | 1 27 ± 02 | 1 046 | 1 33 ± 02 | 110 | f |
| | | 173 | 580 | Ar | 182 | 607 | 1 29 ± 02 | 1 042 | 1 34 ± 02 | 099 | f |
| | | 133 | 508 | Ar | 182 | 540 | 1 29 ± 02 | 1 041 | 1 34 ± 02 | 088 | f |
| | ⊘ | 173 | 580 | He | 577 | 818 | 1 45 ± 02 | < 1 041 > | < 1 51 ± 02 > | 61 | d |
| $O_2$ | ⊠ | 294 | 732 | Ar | 182 | 754 | 1 32 ± 03 | 1 055 | 1 39 + 02 | 127 | f |
| | | 220 | 633 | Ar | 182 | 659 | 1 32 ± 02 | 1 049 | 1 38 ± 02 | 111 | f |
| | | 173 | 561 | Ar | 182 | 590 | 1 35 ± 02 | 1 046 | 1 41 ± 02 | 099 | f |
| | | 133 | 492 | Ar | 182 | 525 | 1 35 ± 02 | 1 042 | 1 41 ± 02 | 088 | f |
| | ◨ | 133 | 492 | He | 577 | 758 | 1 51 ± 05 | < 1 041 > | < 1 57 ± 05 > | 55 | d |
| $CO_2$ | ⊘ | 294 | 707 | Ar | 182 | 730 | 1 28 ± 0 2 | 1 035 | 1 33 ± 02 | 087 | f |
| | ◆ | 294 | 707 | He | 577 | 912 | 1 33 ± 02 | < 1 050 > | < 1 40 ± 02 > | 48 | d |
| $C_2H_4$ | ⊠ | 294 | 782 | Ar | 182 | 802 | 1 32 ± 02 | 1 039 | 1 37 ± 02 | 091 | f |
| Mixed dimers | | | | | | | | | | | |
| NeAr (3 1) | ⊟ | 294 | 699 | He | 577 | 907 | 1 58 ± 02 | < 1 03 > | < 1 63 ± 02 > | 78 | b |
| | | 210 | 591 | He | 577 | 826 | 1 56 ± 02 | < 1 03 > | < 1 61 ± 02 > | 70 | b |
| | | 120 | 447 | He | 577 | 730 | 1 55 ± 02 | < 1 03 > | < 1 60 ± 02 > | 62 | b |
| | ⊠ | 210 | 591 | Ar | 182 | 618 | 1 39 ± 02 | < 1 04 > | 1 45 ± 02 | 099 | a |
| HeNe (3 1) | ⊟ | 31 | 402 | He | 577 | 703 | 1 79 ± 06 | < 1 02 > | < 1 83 ± 06 > | 1 05 | b |
| $H_2Ar$ (8 1) | ⊠ | 90 | 776 | Kr | 204 | 802 | 1 40 ± 02 | 1 04 | 1 45 ± 02 | 10 | f |

*Table VIII 1 Summary of all dimer to monomer cross section ratios investigated* In the second column the symbols are given which are used in fig VIII 1 for the different systems In column $\sigma_2/\sigma_1$ (eff ) the measured ratio of dimer to monomer cross section is displayed these values have to be multiplied by the correction factor $\Delta C_\gamma$ and $\sigma_2/\sigma_1$ (corr ) to obtain the corrected $\sigma_2/\sigma_1$ For the bracketed values of $\Delta C_\gamma$ and $\sigma_2/\sigma_1$ (corr ) the correction is uncertain The column $\hbar v/\varepsilon R_m$ gives the reduced velocity with $\varepsilon R_m$ values for a from ref 7a b from ref 7b, c from ref 7c d from ref 7d e from ref 10 and f from combination rules applied to the ε and $R_m$ values from ref 7a

Fig.VIII.1 shows that at low reduced velocities $v_{red} < .4$, the ratio $\sigma_2/\sigma_1$ assumes values between 1.32 and 1.45, it rises at larger reduced velocities and approaches a value 2 for $v_{red} > 1$. All $\sigma_2/\sigma_1$ results for the large variety of very different systems fall on one single curve in good approximation. Only He forms a striking exception.

For $v_{red} < .4$ the monomer cross section $\sigma_1$ is dominated by attractive forces between monomer and target. With an interaction potential V, $V(r) = -C_{6,m}/r^6$, one has $\sigma_1 = 8.083(C_6/\hbar v)^{2/5}$ (ref.11). When we assume that a similar potential, $-C_{6,d}/r^6$, describes the interaction between dimer and target molecule the ratio $\sigma_2/\sigma_1$ varying from 1.32 to 1.45 points to $C_{6,d}/C_{6,m}$ between 2.0 and 2.5.

Indicated in fig.VIII.1 are the approximate reduced velocities at which glory maxima (integer N) or glory minima (half integer N) would occur in the monomer total collision cross section (ref.12). It is improbable that a loosely bound dimer will survive collisions at glory impact parameters; an eventual glory structure in $\sigma_2/\sigma_1$ will be predominantly due to glories of $\sigma_1$.

No distinct glory structure is observed in $\sigma_2/\sigma_1$; the absence can be explained by the velocity averaging in our experimental set up, by the achieved accuracy for $\sigma_2$ and the smallness of the glory amplitude. For the $H_2$-beam and Ar as target, however, a slight variation of $\sigma_2/\sigma_1$ at $.23 < v_{red} < .58$ is observed, which may be attributed to the N = 1 glory of $\sigma_1$.

For $v_{red} > .8$ (transition region) the repulsive forces determine the monomer cross section. At high reduced velocities, where the "collision diameter" of the constituent monomer becomes comparable to or smaller than the mean distance in the dimer, we expect $\sigma_2/\sigma_1 = 2$.

The ratio $\sigma_2/\sigma_1$ for NO is slightly but significantly lower than for most other systems. This might be attributed to a strong interaction (of chemical nature or due to dipole-dipole forces) between the two NO molecules in the dimer, which decreases the size of the dimer (ref. 13).

A special case is formed by He; for the smallest He-cluster we find a cross section which is 1.95 times the monomer cross section, although the velocity is well within the $v^{-2/5}$-region, $v_{red} = .23$ (Ar as target). This high ratio is one of the arguments by which we have concluded that the smallest cluster observed for He must be a trimer (ref.4).

1. A. van Deursen, A. v. Lumig and J. Reuss, Int. J. Mass Spectrom. Ion Phys., *18* (1975) 129
2. A van Deursen and J. Reuss, to be published, ch. IV of this thesis
3. A. van Deursen and J. Reuss, to be published, ch. VII of this thesis
4. A. P. J. van Deursen and J. Reuss, J. Chem. Phys., *63* (1975) 4559
5. R. B. Bernstein, Comments At. Mol. Phys , *4* (1973) 43
6. J. B. Anderson and J. B. Fenn, Phys. Fluids, *8* (1965) 780
7. a/ J. O. Hirschfelder, C. F. Curtiss and R. B. Bird, "Molecular theory of gases and liquids", Wiley, New York (1965)
   b/ R. Helbing, W. Gaide and H. Pauly, Z. Physik, *208* (1968) 215
   c/ B. N. Srivastava and K. P. Srivastava, J. Chem Phys., *30* (1969) 984
   d/ H. Vehmeyer, thesis, Bonn (1970)
8. F. v Busch, Z. Physik, *193* (1966) 412
   F. v. Busch, H. J Strunck and Ch. Schlier, Z. Physik, *199* (1967) 518
9. R L. Swedenburg, J. A. Phipps, J. E. Scott, Report AEEP-3442-102-70 U, University of Virginia (1970)
10. R. Gengenbach and Ch. Hahn, Chem. Phys., L *15* (1972) 604
11. L. D. Landau and E M Lifshitz, "Quantum Mechanics", Pergamon Press, London (1959)
12. R E. Olson and R. B Bernstein, J. Chem. Phys., *49* (1968) 162
13. P. N. Skancke and J. E. Boggs, Chem. Phys., L *21* (1973) 316

# APPENDIX

## A1. VIBROTOR LEVELS OF DIMERS

In table A1.1 the vibrational levels $\varepsilon_{v,0}$ and rotational constants $B_v$ for $Ar_2$ are shown, taken from Docken and Schafer (ref. A1). The vibrotor levels $\varepsilon_{v,j}$ are given within an accuracy for $\varepsilon_{v,j}/k$ of .2 K (ref.A1) by

$$\varepsilon_{v,j} = \varepsilon_{v,0} + B_v .j.(j+1) \qquad (A1.1)$$

Because $^{40}Ar$ has a nuclear spin I = 0, it behaves like a boson and only even values of j are allowed (see ref. A2). For each vibrational level the largest j value, $j_{v\,max}$, for which a bound state occurs ($\varepsilon_{v,j}<0$) is given in column 4. Alternatively, we calculated the $\varepsilon_{v,0}$ levels for a Lennard Jones 12-6 (L.J.)

table A1.1

| | Ar | | |
|---|---|---|---|
| v | $-\varepsilon_{v,0}/k$ (K) | $B_v/k$ (K) | $j_{v\,max}$ |
| 0 | 120.1 | .083 | 36 |
| 1 | 83.4 | .087 | 32 |
| 2 | 54.4 | .069 | 26 |
| 3 | 32.7 | .062 | 22 |
| 4 | 17.4 | .052 | 16 |
| 5 | 7.8 | .042 | 12 |
| 6 | 2.6 | .030 | 8 |
| 7 | .46 | .017 | 4 |
| 8 | .004 | .003 | 0 |

*Table A1.1 Vibrational levels and rotational constants* for $Ar_2$ from ref A1. The well depth $\varepsilon/k$ = 140.8 K.

interaction potential $V(r) = \varepsilon \{(R_m/r)^{12} - 2(R_m/r)^6\}$ in first order J.W.K.B. approximation by solving the $\varepsilon_{v,0}$ values with $j = 0$ for which v assumes integer values in

$$v + .5 = 2 m_1^{1/2}/h \int_{r_0}^{r_1} [\varepsilon_{v,j} - V(r) - \frac{\hbar^2 j(j+1)}{m_1 r^2}]^{1/2} dr \qquad \text{(A1.2)}$$

Here $r_0$ and $r_1 > r_0$ are the two zero points of the integrand; $m_1$ stands for the monomer mass. It is convenient to write eq. A1.2 in a reduced form

$$v + .5 = 2/\Lambda^* \int_{r_0^*}^{r_1^*} [\varepsilon^*_{v,j} - V^*(r^*) - \frac{\Lambda^{*2} j(j+1)}{4 r^{*2}}]^{1/2} dr^* \qquad \text{(A1.3)}$$

where $r^* = r/R_m$, $r_0^* = r_0/R_m$, $r_1^* = r_1/R_m$, and $\varepsilon^*_{v,j} = \varepsilon_{v,j}/\varepsilon$, $V^*(r^*) = r^{*12} - 2r^{*6}$. The quantity $\Lambda^*$ stands for the reduced de Broglie wavelength† $\Lambda^* = h/R_m (m_1 \varepsilon)^{\frac{1}{2}}$. With $j = 0$ the integral in eq. A1.3 is independent of $\Lambda^*$ and the $\varepsilon_{v,0}$ values depend linearly on $1/\Lambda^*$.

For $Ar_2$ the reduced $\varepsilon^*_{v,0}$ from the L.J. potential with parameters $\varepsilon$ and $R_m$ of ref. A3, are within 1% equal to the $\varepsilon_{v,0}/\varepsilon$ values from ref. A1. Therefore, the $\varepsilon_{v,0}$ values given in table A1.1 are reproduced by our L.J. approximation if we increase at constant $\Lambda^* = .166$ the well depth $\varepsilon$ of the L.J. potential, $\varepsilon/k = 124$ K, to the one from ref A1, $\varepsilon/k = 140.8$ K.

By applying eq. A1.3 one can obtain $\varepsilon_{v,j}$ for $j = 0$ too; however, we aproximate $\varepsilon_{v,1}$ for the L.J. potential according to eq. A1.1 with $B_v = B$ for all vibrational levels. The rotational constant B is taken at the equilibrium distance of the dimer, $B = \hbar^2/m_1 R_m^2$. This approximation yields a value for the partition function $Z_2$ about 15% too small at maximum.

For $^{20}Ne$ the vibrational levels $\varepsilon_{v,0}$ and rotational constants $B_v$ are displayed in table A1.2 taken from the discussion of Tanaka et al. (ref. A4) of UV absorption measurements and their comparison to differential cross section measurements by Siska et al. (ref. A5).

The interaction potential of $(H_2)_2$ does support only the $j = 0$ and $j = 1$ state, with $v = 0$. The energies $\varepsilon_{0,1}$ given in table A1.2 are calculated for a L.J. potential with $\Lambda^* = 1.54$, by directly solving the radial Schrödinger equation for the $H_2$ dimer (ref. A6).

We calculated the vibrational levels $\varepsilon_{v,0}$ for $N_2$ and NO using eq. A1.3 with $\varepsilon/k = 91.5$K, $R_m = 4.132$ Å, $\Lambda^* = .209$ and $\varepsilon/k = 119$K, $R_m = 3.90$Å, $\Lambda^* = .188$, respectively. These values for $\varepsilon$ and $R_m$ are taken from the force constants detemined from viscosity data given in ref. A3. Also indicated in table A1.3 are

† A definition for $\Lambda^*$ used by other authors (see e.g. ref. A3) involves the finite zero point of the potential $\sigma$, instead of $R_m$. The resulting value for a L.J. potential is a factor $2^{1/6}$ larger than the one from our definition.

the maximum rotational quantum number $j_{v\,max}$ using a rotational constant B $= \hbar^2/m_1 R_m^2$ , B/k = .101K for $N_2$, B/k = .105 K for NO. In the calculation of the partition function $Z_2$ the monomer rotational constants $B_a$ are taken from ref. A7, for $N_2$ $B_a/k$ = 2.88 K and for NO $B_a/k$ = 2.44 K.

For the mixed dimer NeAr the $\varepsilon_{v\,0}$ are similarly calculated for a L.J. potential using parameters $\varepsilon/k$ = 65 K, $R_m$ = 3.46 Å, (ref. A8), $\Lambda^*$ = $h/R_m(2\mu\varepsilon)^{\frac{1}{2}}$ = .30 where $\mu$ is the reduced mass. The $\varepsilon_{v\,0}$ value thus found, could be compared to the levels calculated from a more refined potential (see ref. A9). The small effect found for Ar did not seem to justify this effort.

table A1.2

| | $^{20}Ne$ | | | $H_2$ | |
|---|---|---|---|---|---|
| v | $-\varepsilon_{v\,0}/k$ (K) | $B_v/k$ (K) | $j_{v\,max}$ | j | $-\varepsilon_{0\,j}/k$ (K) |
| 0 | 25.3 | .23 | 9 | 0 | 3.7 |
| 1 | 4.3 | .14 | 5 | 1 | 1.4 |
| 2 | .14 | .06 | 1 | | |

*Table A1.2 Vibrational levels and rotational constants* for $^{20}Ne$, from ref A4; the well depth $\varepsilon/k$ = 46K.
*Rotational levels* for $H_2$, from ref. A6; the well depth $\varepsilon/k$ = 34 K, $\Lambda^*$ = 1.54

table A1.3

| | $N_2$ | | NO | |
|---|---|---|---|---|
| v | $-\varepsilon_{v\,0}/k$ (K) | $j_{v\,max}$ | $-\varepsilon_{v\,0}/k$ (K) | $j_{v\,max}$ |
| 0 | 75 | 23 | 99 | 26 |
| 1 | 48 | 18 | 66 | 21 |
| 2 | 28.1 | 14 | 40.5 | 16 |
| 3 | 14.5 | 10 | 22.6 | 12 |
| 4 | 6.0 | 6 | 10.7 | 8 |
| 5 | 1.8 | 3 | 3.6 | 4 |
| 6 | .14 | 0 | .83 | 2 |
| 7 | – | – | <.1 | 0 |

*Table A1.3 Approximate vibrational levels* for $N_2$ and NO for a L.J. 12-6 potential, and maximum allowed quantum number for the end-over-end rotation.

table A2.1

| | 1 | 2 | 3 | 4 | 5a | 5b |
|---|---|---|---|---|---|---|
| $H_2$ | .28 | .28 | .39 | .28 | .30 ± 3% | .35 ± 3% |
| He | .094 | .10 | .13 | .14 | .134 ± 2% | .134 ± 3% |
| Ne | .21 | .24 | .20 | .22 | .258 ± 2% | .230 ± .3% |
| Ar | 1 | 1 | 1 | 1 | 1 | 1 |
| Kr | 1.25 | 1.32 | 1.56 | | 1.34 ± 2% | 1.36 ± 2% |
| Xe | 2.1 | 2.27 | 2.29 | | | |
| $N_2$,NO,$O_2$ | .77 | .82 | .84 | .67 | | |
| $CO_2$ | | | | | .90 ± 3% | 1.01 ± 3% |

*Table A2.1 Relative ionization cross sections* at electron energies 100 and 130 eV (column 1 and 2, see ref A 10) In column 3, 4, and 5 the relative efficiencies are given for ionization gauges from ref A 12a, b, and c, 5a and 5b correspond to different modern gauges, see ref. A11c

## A2 IONIZATION CROSS SECTIONS AND DETECTION EFFICIENCY

In order to compare the monomer intensities for the mixed gases we have tabulated some ionization cross sections with respect to the one of Ar. The electron energies used in the experiment are 100 and 130 eV; in column 1 and 2 of table A2.1 the relative ionization cross sections are given at these two electron energies, taken from ref.A10. At both electron energies the Ar ionization cross section is about 3 $Å^2$ (ref. A11). Experimental data on the relative efficiency for some ionization gauges from literature are given in column 3,4 and 5 (ref.A12).

For noble gas ions Boerboom et al. (ref. A13) have measured the gain of an electron multiplier, similar to the one used in our experiment, at ion energies varying between 3 and 90 keV. They observed the gain to be proportional to $\sqrt{E} - \sqrt{E_0}$, where E is the energy of the ion impinging on the multiplier and $E_0$ is the ion energy at a velocity of $5.5 \times 10^4 msec^{-1}$. In our experiment the ion accelerating voltage is 900 V and the voltage across the multiplier 2 kV. The total ion energy is 2900 V.

Neglecting possible differences in the transmission through the ion optics and the mass magnet, one can calculate the overall relative detection efficiency for Ne compared to Ar from table A2.1 (a relative factor .21) and from the above mentioned multiplier gain (a relative factor 1.26). Our measured ratio of intensity for $Ne^+$ and $Ar^+$, $I_{Ne}/I_{Ar}$, thus indicates that no or very little enhancement of the heavier component occurs in the beam; for a 3:1 mixture Ne-Ar we find $I_{Ne}/I_{Ar} = 0.8 - 1.0$, in the onset region.

A 1 K K Docken and T P Schafer, J Mol Spectrosc , *46* (1973) 454
A 2 see e g N Davidson, "Statistical Mechanics", McGraw Hill, New York (1962)
A 3 J O Hirschfelder, C F Curtiss and R B Bird, "Molecular Theory of Gases and Liquids", Wiley, New York (1965)
A 4 Y Tanaka K Yoshino and D E Freeman, J Chem Phys , *59* (1973) 564
A 5 P E Siska, J M Parson, T P Schafer and Y T Lee, J Chem Phys , *55* (1971) 5762
A 6 J D Poll, private communication
A 7 G Herzberg, "Molecular Spectra and Molecular Structure", D v Nostrand, New York (1954)
A 8 B N Srivastava and K P Srivastava, J Chem Phys , *30* (1969) 984
A 9 C Y Ng, Y T Lee and J A Barker, J Chem Phys , *61* (1974) 1996
A10 A v Engel, "Ionized Gases", Oxford University Press, London (1965), p 63
A11 a/ S Dushman and A H Young, Phys Rev , *68* (1945) 278
b/ Wagener and Johnson, Rev Sci Instr , *28* (1951) 278
identical results have been obtained by G J Schultz, J Appl Phys , *28* (1957) 1149
c/ H G Bennewitz and H D Dohmann, Vakuum Technik, Heft 1, p 8 (1965)
column 5a in table A2 1 is for a gauge IM IV, Leybold-Hereus
column 5b for a gauge type VM IR, Hereus
A12 H S W Massey, E H S Burhop and H B Gilbody, ' Electronic and Ionic Impact Phenomena", Oxford University Press, London (1969), vol I, p 128
A13 B L Schram, A J H Boerboom, W Kleine and J Kistemaker, Physica *32* (1966) 749

In dit proefschrift worden resultaten gegeven van een experimenteel onderzoek aan kleine clusters opgebouwd uit eenvoudige atomen en moleculen

Uit gemeten differentiele botsingsdoorsneden en tweede viriaal coefficienten zijn paar-potentialen te berekenen voor edelgassen welke in goede overeenstemming zijn met U V absorptie metingen, ook zijn bij hoge drukken IR absorptie spectra gemeten van $(N_2)_2$, $O_2Ar$ e a Recentelijk is de bundel resonantie methode toegepast op dimeren die een electrisch dipoolmoment ($(HF)_2$, ArHCl, $(H_2O)_2$, e a ) of een magnetisch dipool moment (KAr, e a ) bezitten

Bij alle niet spectroscopische metingen wordt alleen het massaspectrum gebruikt als indicatie voor het optreden van neutrale clusters Fragmentatie bij detectie wordt of klein verondersteld of geheel verwaarloosd De waargenomen intensiteiten worden geinterpreteerd in termen van een kinetisch of thermodynamisch model voor de vormingsprocessen van kleine clusters

Wij hebben deze assumptie van kleine fragmentatie en de kwantitatieve conclusies betreffende de vormingsprocessen in twijfel getrokken De verzwakking van de neutrale clusterbundel in een verstrooiingskamer moest aantonen of tussen de ionen signalen en bepaalde neutrale clusters een eenduidige correspondentie bestaat Het resultaat is bijna geheel negatief alleen voor dimeren, en dan nog bij zeer lage drukken waarbij het signaal bij de meeste oudere onderzoekingen in de buurt van de detectie drempel ligt, kan men de correspondentie vinden

In hoofdstuk II zijn de in 1973 gepubliceerde eerste resultaten gegeven voor een $H_3$-cluster bundel Door de aanwezigheid van een ionen ruimtelading in de ionisator is hier het dimeer signaal nog niet geheel zuiver

In hoofdstuk III zijn de metingen gegeven aan een Ar clusterbundel waarbij de ruimtelading door zorgvuldige instelling van de massaspectrometer onderdrukt is De intensiteiten van ionen signalen tot en met $Ar_4^+$ zijn gegeven Door onze verstrooiingstechniek is duidelijk aangetoond dat een eenduidig verband tussen neutralen en ionen signalen bestaat voor monomeren en dimeren bij drukken lager dan een grenswaarde $P_1$ Uit de gemeten verzwakking is de botsingsdoorsnede voor $Ar_2$ bepaald

In hoofdstuk IV zijn resultaten gegeven voor Ne, $H_2$, $N_2$, NO en $O_2$ Ook hier zijn de intensiteiten gemeten als functie van brondruk en -temperatuur Voor alle systemen bleek het mogelijk door een reductie van de druk de resultaten voor verschillende temperaturen eenvoudig weer te geven De botsingsdoorsnede is gemeten voor de dimeren ten opzichte van die van monomeren, voor brondrukken lager dan $P_L$

In par IV 4 is een eenvoudige empirische formule gegeven voor $P_1$ , uitgedrukt in gereduceerde grootheden, geldig voor de tot nu onderzochte systemen

Uit de afbuiging van dimeren in een inhomogeen magneetveld kon een magnetisch moment vastgesteld worden voor $(H_2)_2$ en $(O_2)_2$, echter niet voor $(NO)_2$ (par. IV.5). Voor $(H_2)_2$ en $(O_2)_2$ opent dit de mogelijkheid tot bundel resonantie metingen.

In hoofdstuk V geven wij de intensiteiten en verzwakkingen voor een He clusterbundel. Bij lage brondrukken is ook hier een signaal gevonden dat eenduidig toegekend moet worden aan een kleinste cluster, dat hier echter een He trimeer moet zijn.

In hoofdstuk VI gaan we in op de vraag of de dimeren reeds in de bron aanwezig zijn (,,prefabrication'') of in de expansie gevormd worden (,,postfabrication''). De dimeerconcentratie blijkt voorspeld te kunnen worden door een evenwichtsberekening gebaseerd op de aanneming van ,,prefabrication'', binnen een orde van grootte, voor Ar, Ne en $H_2$ zelfs beter. De brondrukafhankelijkheid voor dimeren van $N_2$ en NO wijst echter duidelijk op ,,postfabrication''.

Bundels uit mengsels van gassen zijn beschreven in hoofdstuk VII. Gemengde dimeren NeAr, HeNe en $H_2Ar$ zijn aangetoond en hun botsingsdoorsnede is bepaald.

Tenslotte wordt in hoofdstuk VIII een overzicht gegeven van alle gemeten dimeer botsingsdoorsnedes $\sigma_2$ t.o.v. die van de monomeren $\sigma_1$. Alle $\sigma_2/\sigma_1$ verhoudingen blijken op een universele kromme te liggen, wanneer uitgezet als functie van een gereduceerde snelheid

Bij lage gereduceerde snelheden is $\sigma_2/\sigma_1 \simeq 1.4$, bij hoge snelheden $\sigma_2/\sigma_1 \simeq 2$. De verhouding $\sigma_2/\sigma_1$ bij lage gereduceerde snelheden kan verklaard worden uit een $C_6$ constante voor de dimeren, ongeveer 2.3 maal groter dan die van de monomeren.

Bij hoge gereduceerde snelheden komt de gemeten verhouding $\sigma_2/\sigma_1 = 2$ overeen met de verwachting voor een los gebonden dimeer, waarin de bouwstenen als onafhankelijke botsingspartners beschouwd kunnen worden; bij botsingen met hoge snelheden is hun actieradius vergelijkbaar met of kleiner dan hun onderlinge afstand.

# CURRICULUM VITAE

Op verzoek van het college van dekanen volgt hier een kort overzicht van mijn studie.

In 1965 behaalde ik het diploma gymnasium-β aan het St.-Thomascollege te Venlo en begon mijn studie natuurkunde aan de Katholieke Universiteit te Nijmegen. Het candidaatsexamen werd afgelegd in 1968, het doctoraal examen experimentele natuurkunde volgde in 1971. Een afstudeerstage bij de werkgroep Atoom- en Molecuul fysica, onder leiding van Prof. Dr. A. Dymanus en Dr. J. Reuss ving aan in 1969. Na het doctoraal examen ben ik, in dienst van de stichting Fundamenteel Onderzoek der Materie, aan voornoemde afdeling verbonden als wetenschappelijk medewerker ter voorbereiding van dit proefschrift, onder leiding van Dr. J. Reuss.

Na het candidaatsexamen en ook tijdens het promotie-onderzoek ben ik als assistent werkzaam geweest bij verscheidene werkcolleges alsmede bij het practicum natuurkunde.

Errata

In eq. VI.4 please read $G(kT/\varepsilon)$ instead of $G(Tk_0/\varepsilon)$, in eq. VI.6 $G(kT_0/\varepsilon)$ instead of $G(Tk_0/\varepsilon)$.

Eq. A1.2 should be read

$$v + .5 = \frac{2m_1^{1/2}}{h} \int_{r_0}^{r_1} \left[\varepsilon_{v,j} - V(r) - \frac{\hbar^2 j.(j+1)}{m_1 r^2}\right]^{1/2} dr \ .$$

eq. A1.3

$$v + .5 = 2/\Lambda^* \int_{r_0^*}^{r_1^*} \left[\varepsilon^*_{v,j} - V^*(r^*) - \frac{\Lambda^{*2} j.(j+1)}{4\pi^2 r^{*2}}\right]^{1/2} dr^*$$

on the second line below eq. A1.3 $V^*(r^*) = r^{*-12} - 2r^{*-6}$.

I

Vanwege de grote discrepantie tussen de botsingsdoorsnede voor rotatie-aanslag van $H_2$, berekend met verschillende op het moment bekende anisotropie parameters, is het aan te bevelen deze botsingsdoorsnede in een onafhankelijk experiment te bepalen.

R.J. LeRoy and J. van Kranendonck
J.Chem.Phys. 61 (1974) 4750
L. Zandee, J. Verberne and J. Reuss
Chem.Phys.L. 37 (1976) 1

II

De conclusie van Farrar & Lee dat de translationele energie slechts van geringe invloed is op de snelheid van de reactie $NO + O_3 \rightarrow NO_2^* + O_2$ is niet in overeenstemming met oudere metingen.
Mede gezien deze onzekerheid omtrent de fundamentele processen die in voornoemde reactie een rol spelen, dient men de uiterste voorzichtigheid te betrachten in uitspraken over de resistentie van de atmosferische ozon laag tegen door de mens geproduceerde stikstof oxydes.

J.M. Farrar and Y.T. Lee
Annual Review of Physical Chemistry 1974
A.E. Redpath and M. Menzinger
Can.J.Chem. 49 (1971) 3063

III

Modelberekeningen voor de vorming van dimeren in een supersone bundel zijn slechts zinvol indien rekening gehouden wordt met de interne vrijheidsgraden van de monomeren.

W.G. Dorfield and J.B. Hudson
J.Chem.Phys. 59 (1973) 1253
dit proefschrift

IV

De bewering van Veseth dat de berekening van fijn en hyperfijn interacties voor twee-atomige moleculen met een open schil configuratie, op basis van Hund's case c eenvoudiger zijn en tot een snellere convergentie leiden vergeleken met eenzelfde berekening op basis van Hund's case a, is onjuist.

L. Veseth
J.Phys. B 6 (1973) 1473
L. Veseth
J.Mol.Spectrosc. 59 (1976) 51

V

Bij hun analyse van IR spectra van $H_2$ hebben Gordon & Cashion het j = 1 rotatie-niveau van $(H_2)_2$ ten onrechte, op grond van het vermeende boson karakter van $H_2$, verwaarloosd.

R.G. Gordon and J.K. Cashion
J.Chem.Phys. 44 (1966) 1190

VI

De selectieregel $\Delta|k| = \pm 3n$ voor microgolfovergangen van moleculen met $C_{3,v}$ symmetrie (b.v. $NH_3$) moet vervangen worden door $\Delta k = \pm 3n$.

R.D. Levine and R.B. Bernstein
'Molecular Reaction Dynamics'
Oxford University Press, New York, 1974
T. Oka
J. Chem.Phys. 49 (1968) 3135

VII

Resultaten van berekeningen aan de exchange interactie tussen twee $H_2$ moleculen m.b.v. biorthogonale orbitals moet men op grond van het gebruikte model a priori verwerpen.

E. Kochanski and J.F. Gouyet
Mol.Phys. 29 (1975) 693

VIII

Het begrip atonaliteit kan gebruikt worden ten aanzien van muziek, echter niet voor klank. Waar klanken op zich als muziek aangemerkt worden, geeft dit aanleiding tot een veel voorkomende spraakverwarring.

H. Eimert
'Einführung in die elektronische Musik'
Wergo 60006

Nijmegen, 19-2-1976 A.P.J. van Deursen